An investigation into the reservoir parameters that control induced seismicity in small Dutch gas fields

by

Salima Oumejjoud

4590317

A thesis submitted in partial fulfillment of the requirements for the degree of
Msc Geo-Energy Engineering

Under the supervision of
Dr. A. G. Muntendam-Bos,
Dr. ir. D.J.M. Ngan-Tillard and Dr. ir. F.C. Vossepoel

Faculty of Civil Engineering and Geosciences

Delft University of Technology

12-01-2023

Abstract

Using a field classification, I have assessed the likelihood that a gas field caused a seismic event. I have put the focus on all of the minor gas fields located in the Rotliegend sandstone formation in the Netherlands. These gas fields were divided into five geologically distinctly different regions: the North Holland Platform (NHP), the Groningen Platform (GRO), the Lauwerszee Trough High Pressures (LTHP), the Frisian Platform (FP) and the Lauwerszee Trough (LT). I have investigated which reservoir factors are most influential in deciding whether or not seismicity occurs. The stress ratio has proven to be the most critical parameter. Then, for the stress ratio, I have computed the stress ratio range for each region at which failure will occur. Above the stress ratio, seismic activity will occur, and below the stress ratio, no seismic activity will occur. To answer the research question "Can the reservoir properties of small gas fields in the Netherlands predict the occurrence of seismicity?", I have taken the following steps.

First, I have examined the probability of all small Dutch gas fields being responsible for a seismic event. Based on the distance between the gas field and the nearest event, as well as the presence of other fields in the surrounding area, I have derived a classification for the likelihood that the field was associated with induced seismicity. Second, I have run a sensitivity analysis to identify which parameter was most significant. I have accomplished this by implementing a semi-analytical model that computed and depicted depletion-induced stresses and fault slip along an inclined fault. The model calculated the depletion pressure at which seismic slip starts to occur, here called the onset pressure, based on reservoir data and fault characteristics. The reservoir data contains the compaction coefficient, critical slip weakening distance, dip angle, dynamic friction coefficient, initial reservoir pressure, Poisson's ratio, porosity, reservoir depth, reservoir thickness, shear modulus, static friction coefficient and stress ratio while the fault characteristics included the absolute fault offset and whether the fault is bounding or not.

Afterwards, I have plotted the onset pressure versus the relative fault offset and assessed the sensitivity of the onset pressure whilst changing input parameter settings, namely the critical slip weakening distance, dip angle, dynamic friction coefficient, initial reservoir pressure, Poisson's ratio, porosity, reservoir thickness, shear modulus, static friction and stress ratio. The most critical parameter has turned out to be the stress ratio. I have examined the stress ratio ranges for each field in order to assess whether this parameter could predict the occurrence of seismicity for an entire region. Some fields that do not suit the optimal regional stress ratio have been considered anomalies and investigated further. The main explanations for the anomalies have been geological complexity, assumed synthetic fault offsets, over- or underestimated offsets, unregistered seismic events and substantial overpressure.

The answer to the research question is, yes, it is possible to predict whether seismicity will occur in a small Dutch gas field located in the Rotliegend formation based on reservoir data and fault characteristics. A regional stress ratio has been determined for each of the five regions. The regional stress ratio is 0.51 for NHP, 0.58 for Groningen, 0.69 for LTHP, 0.46 and 0.47 for FP and 0.50 and 0.56 for LT. Salt layers have most likely contributed to higher regional stress ratios for GRO, LT and LTHP.

Acknowledgements

I want to express my gratitude to Annemarie Muntendam-Bos, my chair supervisor, for all of her guidance, assistance and support. She created the idea for the thesis and helped me to participate in this research. Additionally, I want to thank Dominique Ngan-Tillard and Femke Vossepoel, my supervisors, for their excellent counsel, support and consideration. I also want to express my gratitude to my family and friends for supporting me. Finally, I want to specifically thank my best friends Nisha, Daphne and Kirina for their unwavering support, care and encouragement.

Contents

1 Introduction

The gas extraction in Groningen has caused earthquakes, which led to significant societal and environmental problems. Residents are angry because their homes have been damaged or lost. People are also concerned about the impact of the gas projects on the Wadden Sea, which is a national nature monument. The Dutch government decided in 2018 that gas production from the Groningen Gas Field (GGF) must be ceased. The plan was to begin reducing gas production in 2019-2020 and end in 2023 or 2024 at the latest. GGF is the largest gas field in the Netherlands, which has been of great economic value. The produced gas is utilized as an energy source, for example, to heat houses, and it is also exported and stored. Moreover, it has helped make the Netherlands self-sufficient in its energy provision. The remaining gas sources, which are smaller onshore and offshore gas fields, have become more important. But their production could also be halted if these result in frequent or powerful earthquakes. Consequently, in order to avoid this, an analysis will be performed to predict the occurrence of seismicity based on reservoir parameters. Onshore and offshore gas exploration occurs predominantly in the northern part of the Netherlands. Offshore gas fields are outside of the scope of this study because determining seismicity offshore with sufficient accuracy is challenging and the faraway fields beyond about more than 20 km do not directly impact citizens and their homes. Another issue associated with gas depletion is subsidence, which is beyond the scope of this study. The Rotliegend sandstone formation, which was chosen because it is the source of most seismicity, contains all of the gas fields that were analysed (Muntendam-Bos, 2021).

Since 1996 onshore gas fields are being monitored in order to detect any seismicity. Important factors that control the occurrence of seismicity for gas fields in the Netherlands have been the focus of several studies. The sensitivity for fault activation due to differential compaction relies on the fault-reservoir geometry, according to research done by Roest & Kuilman (1994). Later Van Eijs et al. (2006) found three crucial factors that affect seismicity, namely pressure drop, reservoir fault density and stiffness ratio between seal and reservoir rock. Buijze et al. (2017) used numerical geomechanical modeling to determine how gas production affects the forces in the subsurface. The results showed that fault behavior and reservoir initial stress had an effect on the magnitude of the seismic event. Moreover, the geometry of the faults and the gas reservoir play a significant role in the occurrence of seismic events. According to Van Thienen-Visser et al. (2018), inter-reservoir offset faults require less reservoir depletion to reach failure than bounding faults and faults with a small offset. According to Muntendam-Bos (2021), the stress changes on the offset faults are insufficient to explain the seismicity. The presence of the visco-elastic evaporite rocks of the Zechstein formation has a significant impact on the in-situ stress field and on the fault stability. A study done by Leltz (2022) delves into how salt can affect the state of stress depending on where the salt is in relation to the reservoir layer.

Seismically active gas fields can have serious safety, financial, and environmental consequences. When they must be abandoned, there are financial ramifications for the operating company. This study shows how seismicity can be predicted using reservoir data before any production begins, thereby minimizing these major consequences.

The goal is to determine if a field could become seismically active or not based on the reservoir parameters of smaller onshore gas fields. The research question is, "Can the occurrence of induced seismicity be predicted using reservoir parameters for smaller gas fields in the Netherlands?"

The geological background is covered in the chapter 2. In chapter 3 the history of induced earthquakes in the Netherlands is presented. Chapter 4 explains the geomechanical background. The approach is discussed in chapter 5. Chapter 6 describes the sensitivity analysis. Chapter 7 shows the results, which is followed by a discussion in chapter 8 that includes the uncertainties. A conclusion is provided in chapter 9.

2 Geological background

The source rock of the gas in the Dutch gas fields is the Carboniferous formation. The Lower Cretaceous sandstones, the Lower and Upper Triassic sandstones, the Zechstein carbonates, the Carboniferous limestones and the Rotliegend sandstones are all the formations where this gas was trapped after it migrated upwards (Muntendam-Bos, 2022). Information about these groups are provided in order to have a better understanding of the geology. Despite the fact that the Rotliegend group is the focus of this study, the other formations have an impact on the reservoir conditions. The cross-sections in figure 1 help to understand the structural geology and the stratigraphical groups that are present. The location of the cross sections is indicated in figure 2. The West Netherlands Basin has a relatively high fault density over all the groups. The entire Lower and Upper Rotliegend groups exhibit faults across the cross section. The cross section also displays the varying dips and thicknesses of the layers.

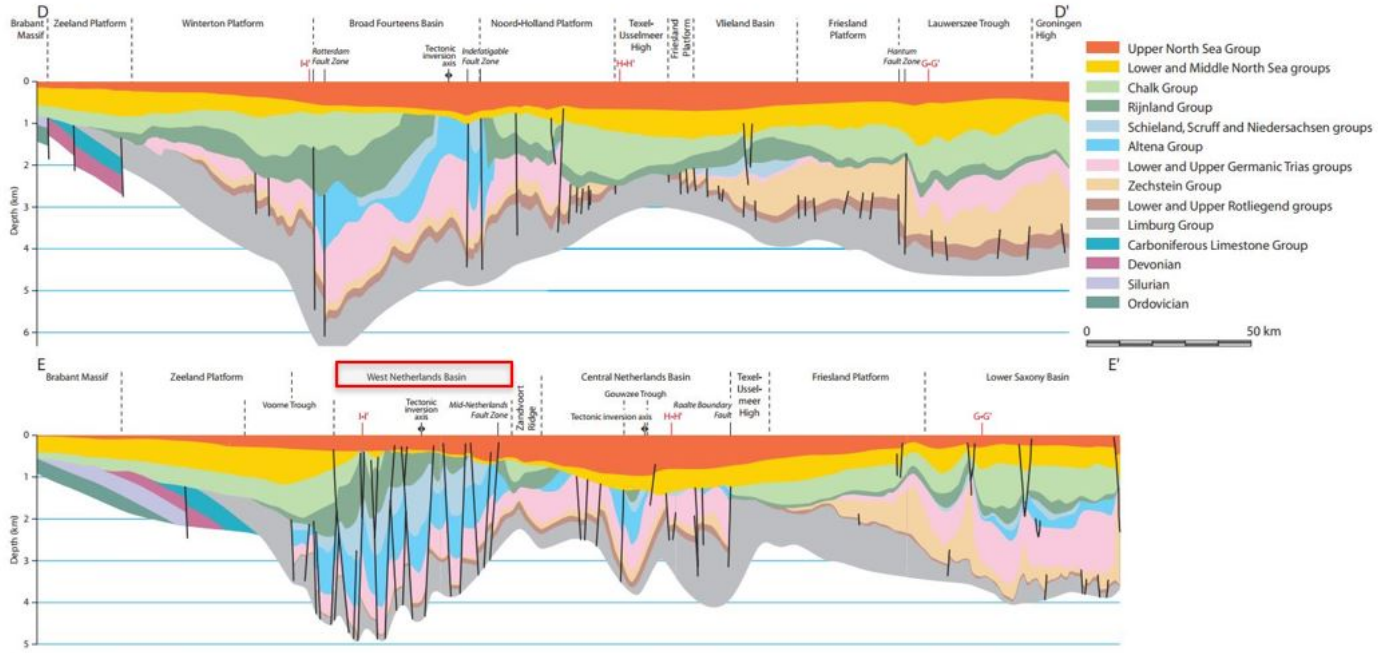

Figure 1: Two NE-SW cross-sections of the Netherlands (Duin et al., 2006)

Figure 2: Position of intersections in the overhead view (Duin et al., 2006)

2.1 Carboniferous Coal

The coal layers of the Carboniferous formation are the source of the gas found in the Dutch gas fields (Muntendam-Bos, 2022). These were formed in the Carboniferous period, which started roughly 360 million years ago and ended 300 million years ago. The Netherlands was located close to the equator during this period (Kombrink, 2008). In this period, there were warm seas, mangrove swamps and river deltas. The high concentration of CO2 made extensive vegetation on the land possible. In the swamps peat was created which was later turned into coal. The top of the Carboniferous can be more than 6000 metres deep, and local Carboniferous deposits can be up to 4000 metres thick (TNO-NITG, 2004). Although the coal was buried far below the surface, it still produced gas as a result of its burial (Kombrink, 2008).

In the southern part of the Dutch onshore and offshore these sediments consist of black limestones whereas in the northern offshore Early Carboniferous rocks are of clastic origin. Upper Carboniferous deposits (Namurian, Westphalian and Stephanian) are widely distributed in the subsurface of the Netherlands (Van Adrichem Boogaert & Kouwe, 1993-1997). The total thickness and distribution of the Carboniferous strata is not known in detail due to their deep burial (Mijnlieff, 2005). The depth of the top of the Carboniferous can be greater than 6000 m and the Carboniferous deposits locally reach thicknesses of more than 4000 m (TNO-NITG, 2004). In many locations these deposits are thicker than the total thickness of the cumulative Permian to Cenozoic deposits.

2.2 Rotliegend sandstones Group

The Lower and Upper Rotliegend sediments were deposited under continental conditions during the Early and Middle Permian in the Southern Permian Basin (SPB), see figure 3a. The majority of the Netherlands has been filled with part of the basin and was filled in the Upper Rotliegend with mainly eolian and fluvial sediments, see figure 3b. The entire SPB is the result of the amalgamation of three basins, namely Anglo-Dutch Basin, North German Basin and Polish Trough. These basins have different geological histories. Despite the fact that the lithosphere's thermal relaxation is primarily what causes their subsidence (Ziegler, 1990a; Gast & Gundlach, 2006; Van Wees et al., 2008).

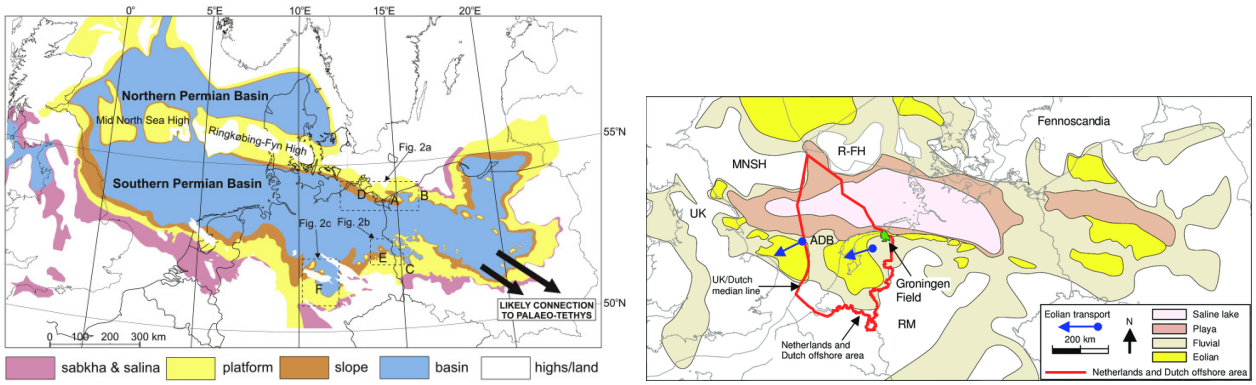

(a) Northern and Southern Permian basin(Slowakiewicz et al., 2017)

(b) SPB facies of Upper Rotliegend sandstone (Mckie, 2011)

Figure 3: Zechtstein Group depositional location

The presence of the Rotliegend and Zechstein deposits characterises the Southern Permian Basin. In the G-block in the northeastern offshore area, as shown in figure 4 (Geluk, 2005), the thickness of the Rotliegend section reaches a maximum value of more than 900 m (Duin et al., 2006). The study area is only for a small portion included in the depocentre area according to figure 4. The Southern Permian Basin has grown in a WNW-ESE direction. In the Southern Permian Basin, erosion caused by the Jurassic is the reason that the Rotliegend deposits are not present locally (Duin et al., 2006).

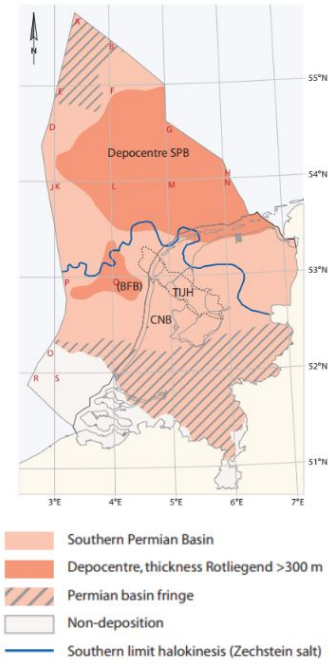

Figure 4: Depocentre SPB (Geluk, 2005)

2.3 Zechstein Group

The Southern Permian Basin's southern boundary is defined by the location of the southernmost Zechstein sediments. The outlines of the Zechstein basin coincide largely with the occurrence of deposits of the Upper Rotliegend Group, see figure 4. The Zechstein is formed in the Middle to late Permian. The current depth of the Zechstein Group's base varies from about 700 metres in the southeast of the Netherlands to more than 5000 metres in the Dutch Central Graben, the Broad Fourteens Basin, and the West Netherlands Basin, see figure 1. Due to shallow

basin development, only thin Zechstein deposits are found in the southern Netherlands.

The salt is a product of the evaporation of the Zechstein sea, see figure 5a. Figure 5b shows the location of the deposition of salt. The Zechstein group can be separated in several formations, see figure 6. The figure also shows the difference in between the general stratigraphy of the Netherlands versus Germany. The lithologies are salt, anhydrite, dolomite, limestone and clay-/siltstone. Germany contains more formations and is largely similar to the Netherlands. The only difference is that Z1 Germany contains more salt.

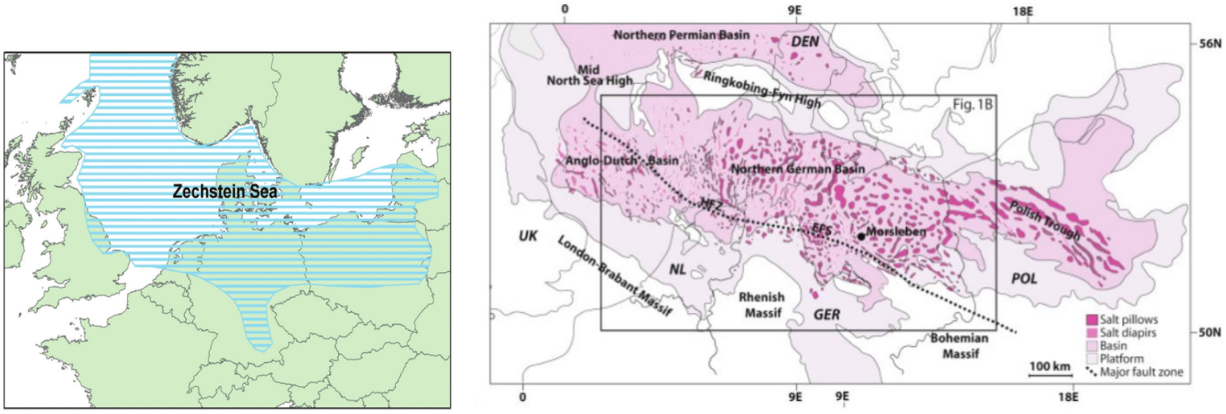

(a) Zechstein sea location, beta 260-248 Myr (Doyle, 2008)

(b) Location of salt deposition in SPB

Figure 5: Zechtstein Group depositional location

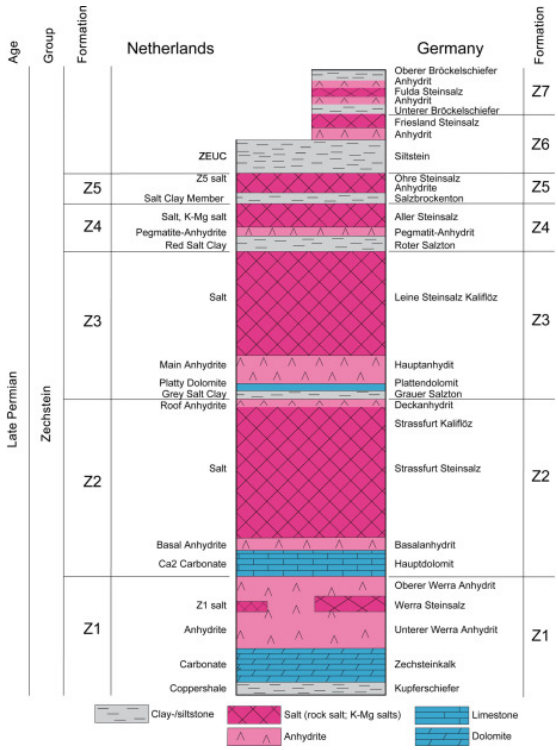

Figure 6: Stratigraphy of the Zechstein formations, Netherlands & Germany (Strozyk et al., 2017)

The depth map of the Zechstein Group's base in figure 7a clearly shows the locations of basins that further subsided during the Early and Late Kimmerian phases, such as the Dutch Central Graben. The Zechstein is absent due to Mid- and Late Kimmerian erosion at the Maasbommel, Winterton , Texel-IJsselmeer, Dalfsen and Elbow Spit

highs. On Late Jurassic platforms, the Zechstein Group's thickness increases significantly to the north, reaching a maximum of more than 900 m, see figure 7b.

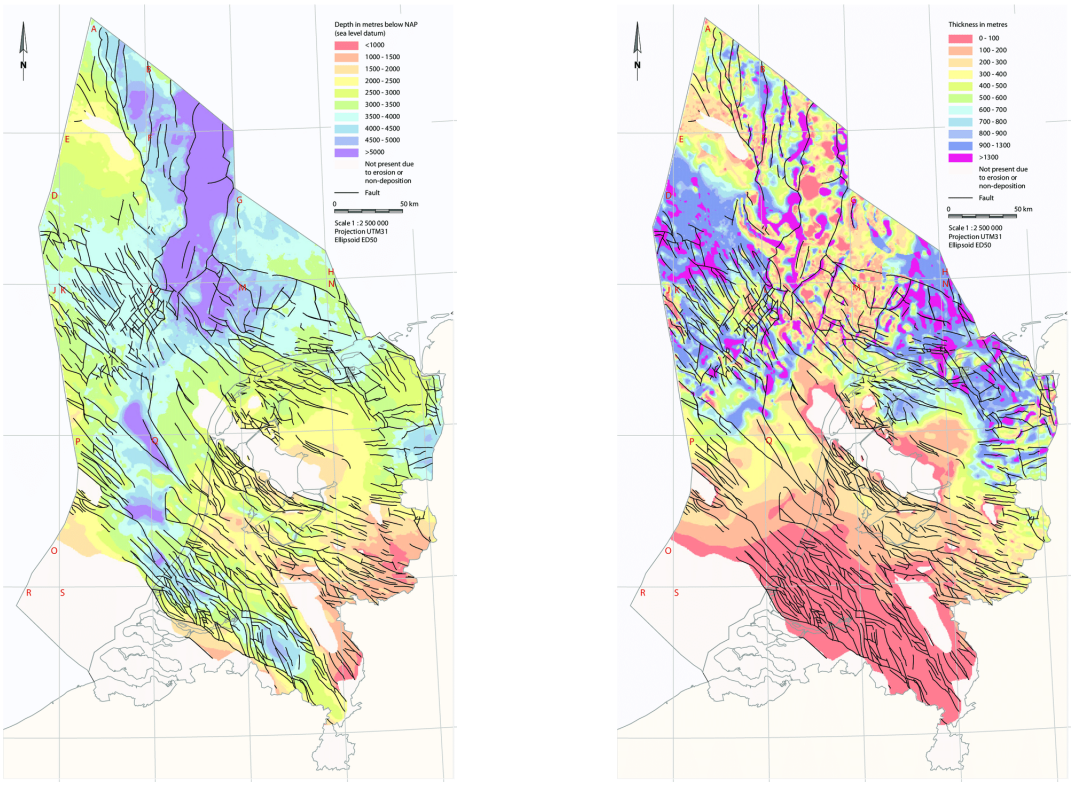

(a) Depth of Zechstein Group (Duin et al., 2006)

(b) Thickness of Zechtstein Group (Duin et al., 2006)

Figure 7: Zechtstein Group

The Dutch Central Graben and the Terschelling Basin show pronounced occurrences of salt diapirs and walls. Salt structures with local thicknesses of more than 1300 m are frequently found in the northeastern onshore and northern offshore areas, see figure 7b. The lateral thickness variations make the area of mobilised Zechstein salt very obvious. In tectonically active areas, such as the Terschelling Basin, the thickness of the original Zechstein deposit is obscured by salt movement. Additionally the salt was able to act as a seal due to its large thickness and viscous nature.

2.4 Germanic Trias Group

In the Triassic the Germanic Trias group was created. Currently, the Dutch Central Graben has a base depth of the Lower Germanic Trias Group that is over 5000 m deep, see figure 8. In eastern Netherlands, this depth is about 500 metres. In the Roer Valley Graben, Terschelling, Broad Fourteens, Central Netherlands, and Lower Saxony basins, thick Triassic deposits have been preserved as a result of Jurassic subsidence. The Dutch Central Graben, Roer Valley Graben, and Broad Fourteens Basin all experienced relatively faster subsidence during the Triassic period than the surrounding regions, resulting in greater thicknesses in these basins (Geluk, 2005). The faults in the Triassic are the result of rifting in the Jurassic and inversion tectonics in the Late Cretaceous (Ziegler, 1988). Normal faults in inversion tectonics provide a pre-existing plane of weakness that is then reactivated as a reverse fault during contraction (Kortyna et al., 2019). The uplift of the sedimentary layers are the result of crustal shortening. The convergence of Europe and Iberia is the cause of inversion tectonics (Voigt et al., 2021). Additionally, erosion and salt walls prevented faulting.

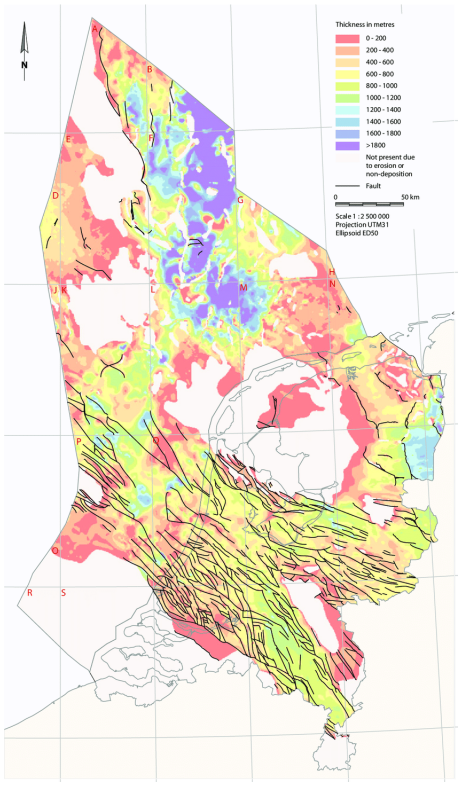

Figure 8: Thickness of Upper and Lower Germanic Trias Group (Duin et al., 2006)

2.5 Rijnland Group

The Broad Fourteens and West Netherlands basins are the locations of the Lower Cretaceous depocentres on the Rijnland Group thickness map, see figure 9b. Minor depocentres were formed in the Vlieland, Terschelling, and Lower Saxony basins. The Roer Valley Graben, Central Netherlands Basin, and Dutch Central Graben were affected by the erosion of Rijnland deposits. The depth of the Rijnland Group ranges from the outcrops in the eastern part of the Netherlands to more than 3000 m in the A- and B-blocks, which is partially caused by the North Sea Basin's significant basin subsidence during the Cenozoic, see figure 9a. About 75% of the recorded subsidence in the most recent Cenozoic period, the Quaternary, is caused by compaction and load-induced subsidence (Arfai et al., 2018).

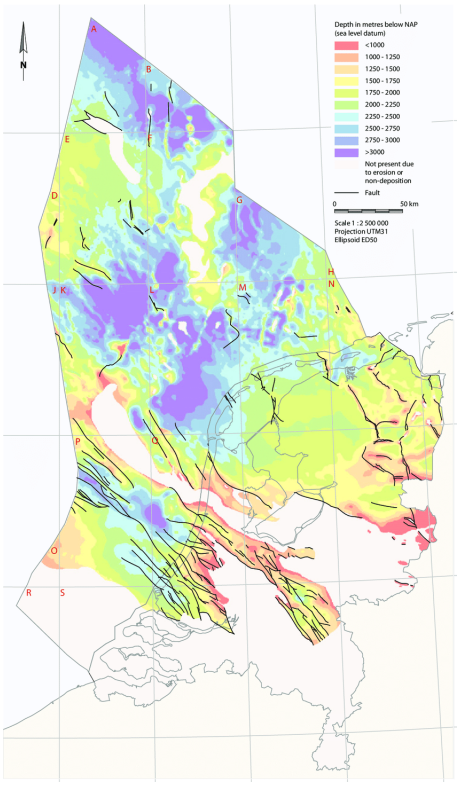

(a) Depth of Rijnland Group (Duin et al., 2006)

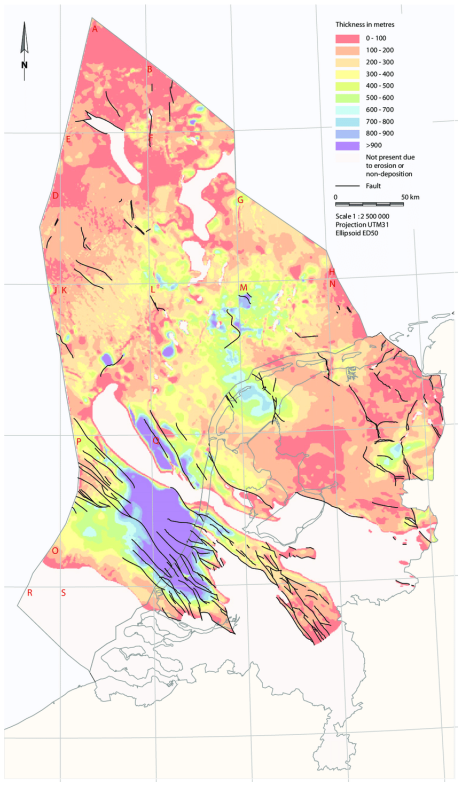

(b) Thickness of Rijnland Group (Duin et al., 2006)

Figure 9: Rijnland Group

3 History of induced seismicity

Figure 10 shows all the seismic events that have occurred in the Netherlands along with their magnitude. The north-east is dominated by induced events, while the south-east is dominated by tectonic events. In 1986 the first induced seismic event was recorded by The Royal Netherlands Meteorological Institute (KNMI) with a magnitude (M) of 2.8. The event took place in Assen and was later assigned to the Eleveld gas field (Muntendam-Bos et al., 2022).

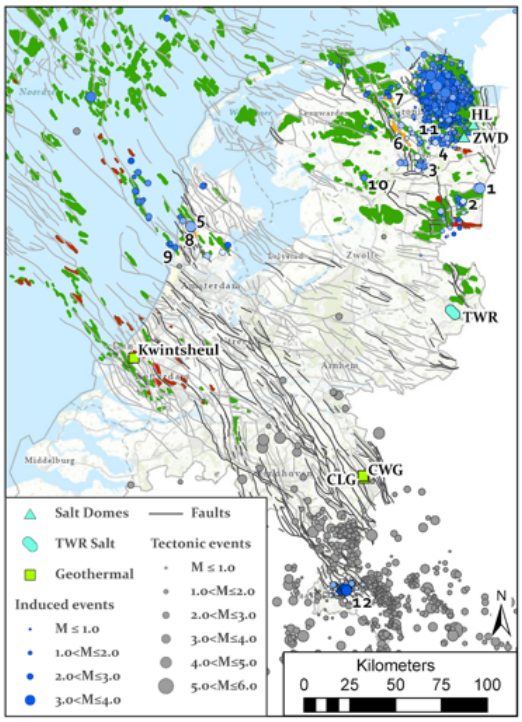

Figure 10: Seismic events in the Netherlands (Muntendam-Bos et al., 2022)

Figure 10 shows all the oil fields in red. The oil production is much less extensive in comparison to the gas production. Currently about 15 oil fields are in production (Oil and gas | NLOG, n.d.), which includes on- and offshore. Schoonebeek in Drenthe is an oil field which is the second largest onshore field of West Europe (Herber & De Jager, 2010).

The green fields in figure 10 represent the gas fields. In total the Netherlands has about 240 gas fields next to Groningen, about half of that is located in the North Sea. The gas reservoirs are located in Groningen, Friesland, Overijssel, Noord-Holland, Zuid-Holland, Noord-Brabant, North Sea and the Wadden Sea (Ministerie, 2021). These reservoirs are predominantly located in the Rotliegend sandstone overlain by Zechstein salt and others are located in a carbonate layer in the Zechstein formation and sandstone layer in the Triassic and Lower Cretaceous formations (Muntendam-Bos, 2022). The only gas fields that have led to seismic events with a magnitude (M) larger than 3.0 are Roswinkel (M=3.4), Bergermeer (M=3.5) and Groningen (M=3.6) (Muntendam-Bos et al., 2022).

Most of the induced seismic events have taken place in Groningen as shown in figure 10. The Groningen gas field is the largest gas field in Europe (Whaley, 2009). The gas reservoir is located in the upper Rotliegend Group. The field was discovered in 1959 and in 1963 production started (Groningen gasveld | NLOG, n.d.). The first recorded event (ML = 2.4) in the Groningen gas field occurred in December 1991 (van Thienen-Visser & Breunese). The province Groningen had an earthquake with the largest magnitude of 3.6 in Huizinge in August 2012 (Dost & Kraaijpoel, 2013). After this event the amount of earthquakes with a magnitude larger than 1.5 have been decreasing due to production limitations as can be seen in figure 11 (KNMI - Aardbevingen door gaswinning, n.d.). Overall, the Groningen gas field has led to more than 1400 seismic events up until 2022 (Muntendam-Bos et al., 2022). While the majority of those events have a moderate magnitude, the frequency is very high.

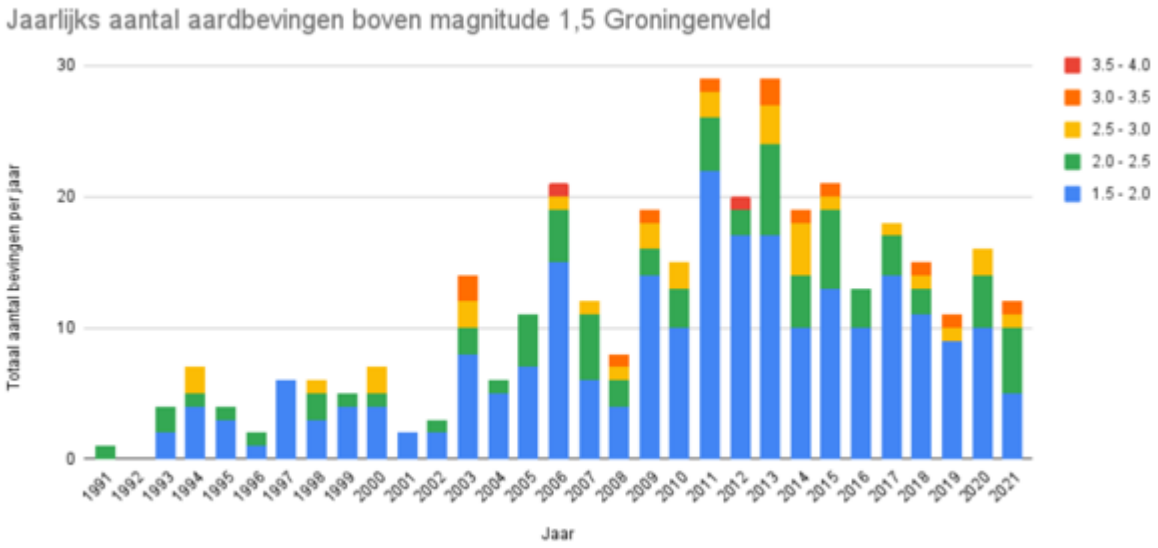

Figure 11: Yearly total earthquakes in GGF with a magnitude larger than 1.5 (KNMI - Aardbevingen door gaswinning, 2022)

KNMI is in charge of weather forecasting as well as weather, climate, air quality and seismic activity monitoring (KNMI, n.d.). In 1904 KNMI started with seismic monitoring in de Bilt with the first measuring station (KNMI, n.d.). Generally speaking magnitudes lower than 1.5 on the scale of Richter can not be felt by humans and have minimal impact. Other factors, like depth and soil characteristics play a significant role in determining the impact of an event and cannot be determined solely by magnitude. However, events with a magnitude of 1.5 to 2.0 may be felt by the general public in the Netherlands because of the soft top soils and shallow hypocentres (Muntendam-Bos et al., 2022). Additionally in the years 2014-2015 the KNMI extended their monitoring network with significantly more geophones and accelerometers. Hence, now it is possible to measure all events with magnitudes 1.0-1.5 and more of the events 0.5-1.0 (KNMI, n.d.). Figure 12 depicts the seismic network in 2020, along with the magnitudes and extents that can be measured.

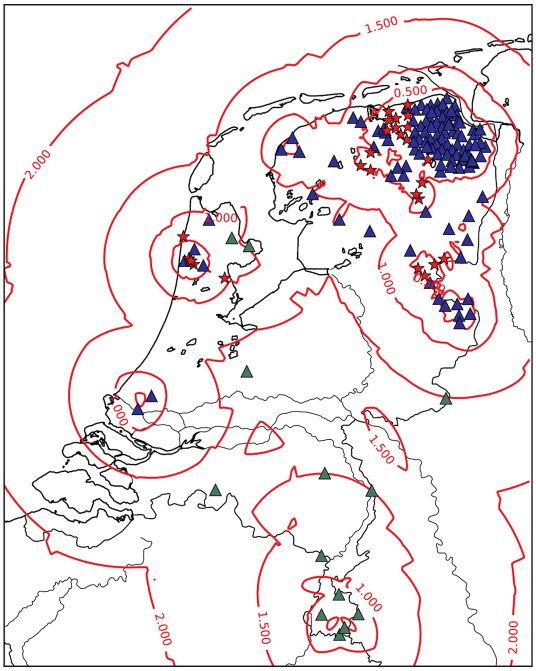

Figure 12: Overview of the Dutch national seismic network station locations (triangles) and location thresholds (annotated red lines) (June 2020; credit KNMI). The blue triangles represent the 200 m deep borehole stations, which are made up of four seismometers spaced at 50 m intervals. The surface broadband stations are represented by green triangles, whereas the surface accelerometers are represented by red stars (Muntendam-Bos et al., 2022).

4 Geomechanical background

As gas is produced, the pore pressure within the rock drops. A portion of the load was previously carried by the gas in the pores of the reservoir. As the pore pressure reduces more and more weight of the overburden needs to be carried by the rock matrix, which causes the rock to become compacted (De Waal et al., 2012). Compaction can lead to subsidence, which is a process that is out of the scope of this report as previously mentioned. Additionally, the decrease in the pore pressure also influences the state of stresses on faults. Since there is a normal faulting regime at the moment, the horizontal stress is the smallest and the vertical stress is the largest. The Mohr circle widens as a result of depletion, because there is a larger increase in the vertical stresses than in the horizontal stresses assuming poro-elasticity, see figure 13 (Altmann, 2010). Thereby making it easier for the fault to hit the failure envelope and become reactivated. However this only applies to some reservoirs and is dependent on the Poisson's ratio. Fault slip will occur if the shear stress exceeds the frictional force. Based on research from Van den Bogert (2018), the slip will be aseismic unless the slip distance exceeds a critical slip distance; this will be explained in greater detail later in this chapter.

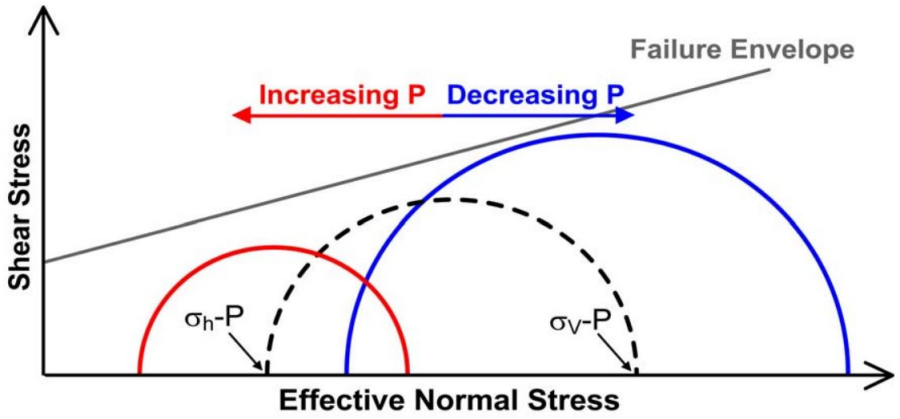

Figure 13: Change in Mohr circle due to pressure de- and increase

Figure 14 depicts an overview of all the processes, which will be further explained in this chapter.

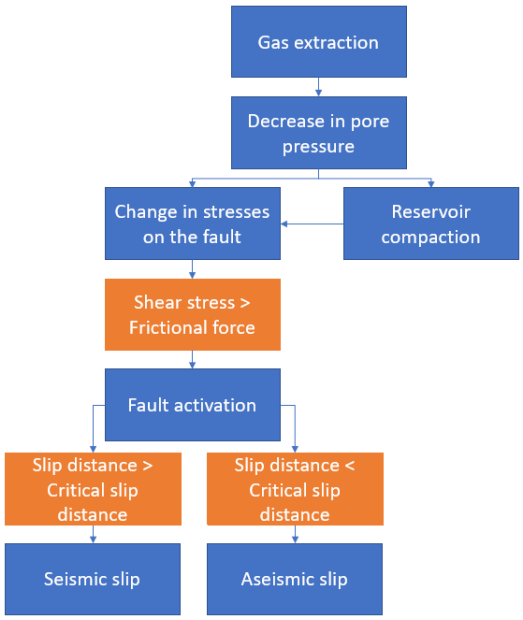

Figure 14: Overview of processes that affect induced seismicity

4.1 Elastic stresses

The semi-analytical model developed by Jan-Dirk Jansen and Bernard Meulenbroek is based on equation 1 defined by Jansen et al (2019), which describes the incremental stresses inside and outside the reservoir due to depletion.

$$\sigma_{ij}(x,y) = \iint_{\Omega} C(\zeta,\xi) g_{ij}(x,y,\zeta,\xi) d\Omega - C(x,y) 2\pi d_{\Omega} \tag{1}$$

The first part of the equation is a double integral of C and g_{ij}. x and y are the 2D Cartesian coordinates, while ζ and ξ are the coordinate values within the reservoir layer Ω, which is the permeable inclusion where the pressure is decreasing. The g_{ij} term contains Green's functions for the incremental stresses (Jansen et al, 2019). The second part of equation 1 is based on C with x and y coordinates and a modified form of the Kronecker delta, which is described in equation 2 (Jansen et al, 2019).

$$d_{\Omega} = \begin{cases} 1 & \text{if (x,y)} \in \Omega \\ 0 & \text{if (x,y)} \notin \Omega \end{cases} \tag{2}$$

The dimensionless function C is defined in equation 3 (Jansen et al, 2019), it contains the Poisson's ratio (ν), Biot's coefficient (α), incremental pore pressure in the reservoir as a function of location ζ and ξ (p) and bulk modulus (K). The Biot's coefficient denotes the ratio of the volume of fluid change divided by the change in bulk volume when pore pressure remains constant (Raziperchikolaee et al., 2020).

$$C(\zeta, \xi) = \frac{(1 - 2\nu)\alpha p(\zeta, \xi)}{2\pi(1 - \nu)} \tag{3}$$

The remaining equations in this sub-chapter are based on a reservoir model that is shown in figure 15. The x and y direction are defined in the figure. The width of the reservoir in the x direction is infinitely long. The $\hat{x}$ is along the fault line and perpendicular to the $\hat{y}$. The thickness of the reservoir is the sum of a and b. The absolute offset of the reservoir layer of the fault can be defined by subtracting a from b and the relative offset by equations 4 and 5. The fault dip angle is defined as θ. Note that for the following equations ^{0} stands for the initial stress and ' for effective stress. It is critical to understand that gas production can reactivate faults and cause them to slip. Table 1 contains symbols that will be used in the following equations.

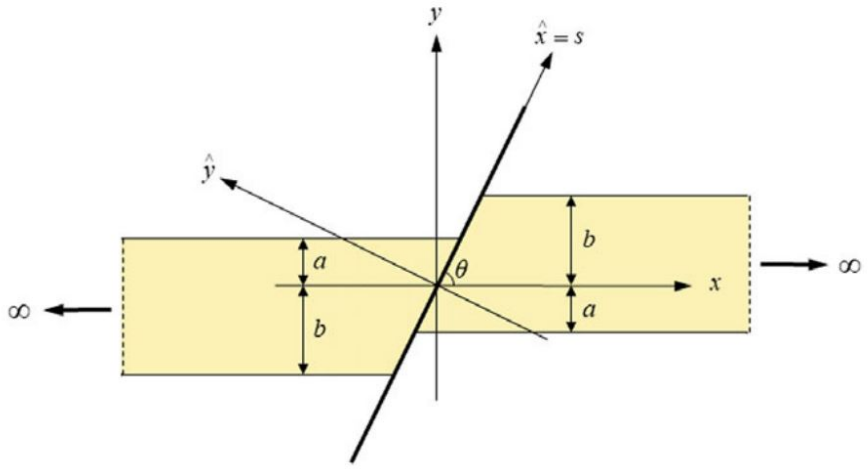

Figure 15: Reservoir geometry (Jansen & Meulenbroek, 2022)

$$\text{Relative offset} = \frac{|\text{Vertical offset}|}{\text{Reservoir thickness}} \tag{4}$$

$$\text{Relative offset} = \frac{|b - a|}{a + b} \tag{5}$$

Table 1: Symbols

Symbol	Description
g_{ij}	Green's functions for the incremental stresses
ν	Poisson's ratio
α	Biot's coefficient
K	Bulk modulus
θ	Fault dip angle
p	Reservoir pressure
μ	Friction coefficient
$\Sigma_{\|\|}$	Total shear stress
Σ_{sl}	Slip threshold
k	Cohesion
$\sigma_{\|\|}$	Incremental shear stress
$\Sigma'_{\perp}$	Total effective normal stress
$\sigma_{\perp}$	Normal stress

Slip occurs when the absolute slip threshold is exceeded by the absolute total shear stress along the fault, see equation 6.

$$|\Sigma_{||}| > |\Sigma_{sl}| \tag{6}$$

The total shear stress along the fault is the absolute sum of the initial shear stress and incremental shear stress, see equation 7 below. The initial and incremental shear stress are defined in equations 8 and 9.

$$\Sigma_{||} = \sigma^0_{||} + \sigma_{||} \tag{7}$$

$$\sigma^0_{||} = -\sigma^0_{\hat{x}\hat{y}} = (\sigma^0_{xx} - \sigma^0_{yy})sin(\theta)cos(\theta) \tag{8}$$

$$\sigma_{||} = \sigma_{xy}sin^2(\theta) + \sigma_{xx}sin(\theta)cos(\theta) \tag{9}$$

The slip threshold is defined by equation 10, where k stands for the cohesion which is always positive or zero and μ for the friction coefficient. The last parameter Σ' stands for the total effective normal stresses and is described in equation 11. The sum of the effective normal stresses are described by the initial and incremental normal stresses.

$$\Sigma_{sl} = \kappa - \mu\Sigma'_{\perp} \tag{10}$$

$$\Sigma'_{\perp} = \sigma'^0_{\perp} + \sigma'_{\perp} \tag{11}$$

The initial normal stresses and initial effective normal stresses are defined by equations 12 and 13. The initial effective normal stresses depend on the dip angle, initial stress in the vertical and horizontal direction, the effective stress coefficient for fault friction (β) and initial reservoir pressure (p^0).

$$\sigma'^0_{\perp} = \sigma^0_{\perp} + \beta p^0 \tag{12}$$

$$\sigma^0_{\perp} = \sigma^0_{\hat{y}y} = \sigma^0_{xx}sin^2(\theta) + \sigma^0_{yy}cos^2(\theta) \tag{13}$$

The incremental effective normal stresses partially depend on incremental normal stresses. Additionally, it was assumed that the relevant fault segment is represented by -b<y<b and that incremental reservoir pressure only occurs along those portions of the fault that are in direct contact with the reservoir. The domain where βp is introduced should be expanded if a bigger portion of the fault is exposed to incremental pressure (Jansen & Meulenbroek, 2022). Moreover, the incremental normal stresses depend on the dip angle (Jansen & Meulenbroek, 2022).

$$\sigma'_{\perp} = \sigma_{\perp} + \begin{cases} 0 & \text{if y} \leq \text{-b or b} \leq \text{y} \\ \beta p & \text{if -b<y<b} \end{cases} \tag{14}$$

$$\sigma_{\perp} = -\sigma_{xy} sin(\theta) cos(\theta) + \sigma_{xx} sin^2(\theta) \tag{15}$$

Now the theory of slip weakening will be discussed. This theory assumes that the friction coefficient reduces linearly during slipping until it reaches the reduced friction coefficient, see figure 16. At that moment the critical slip distance is reached and seismicity will occur. After reaching this point the friction coefficient does not decrease any more, but remains constant at the reduced friction coefficient also known as the dynamic friction coefficient (μ_{dyn}), see figure 16. Here W_{μ} represents the absolute friction coefficient reduction per millimetre of relative slip displacement over the fault. The relative slip displacement is the slip displacement along the fault line relative to the reservoir thickness.

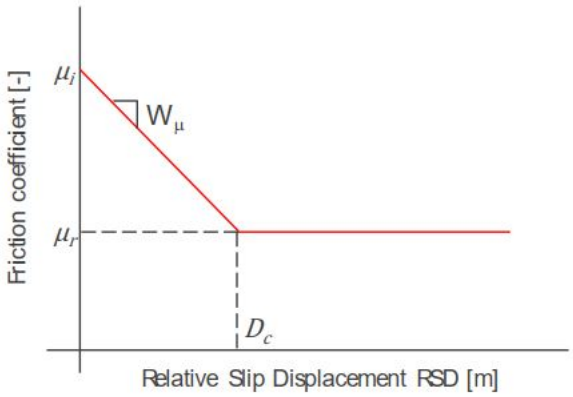

Figure 16: Slip weakening slope (Van den Bogert, 2018)

So the previously mentioned slip threshold in equation 9 must be redefined with equation 16, because the friction coefficient is not a constant in the theory of slip weakening (Jansen & Meulenbroek, 2022). The slip stress is equal to the effective normal stresses multiplied by a term that depends on the slip distance. If the slip distance (δ) is larger than the critical slip distance (δ_c) then the term is equal to the dynamic friction coefficient (μ_{dyn}). Otherwise it depends on the dynamic and static friction coefficient (μ_{st}), absolute slip distance and critical slip distance.

$$\Sigma_C(y, \delta(y,p), p) = \Sigma_{||}(y,p) - \Sigma_{sl}(y, \delta(y,p), p) = \Sigma_{||}(y,p) - \Sigma'_{\perp}(y,p) \cdot \begin{cases} \mu_{st} - (\mu_{st} - \mu_{dyn}) \frac{|\delta(y,p)|}{\delta_c} & \text{if } |\delta(y,p)| \leq \delta_c \\ \mu_{dyn} & \text{if } |\delta(y,p)| > \delta_c \end{cases} \tag{16}$$

Van den Bogert (2018) shows with figure 17 that the pressure depletion at which seismicity can occur strongly depends on the normalised offset and slope W_{μ}. Figure 17b shows that as the slope W_{μ} increases, the reservoir depletion required to cause a rupture or slip decreases and the O symbol in the legend stands for the normalised offset. Moreover, larger normalised offsets need less pressure depletion to rupture or slip. In chapter 6 I will assess these sensitivities for the Dutch gas fields in more detail.

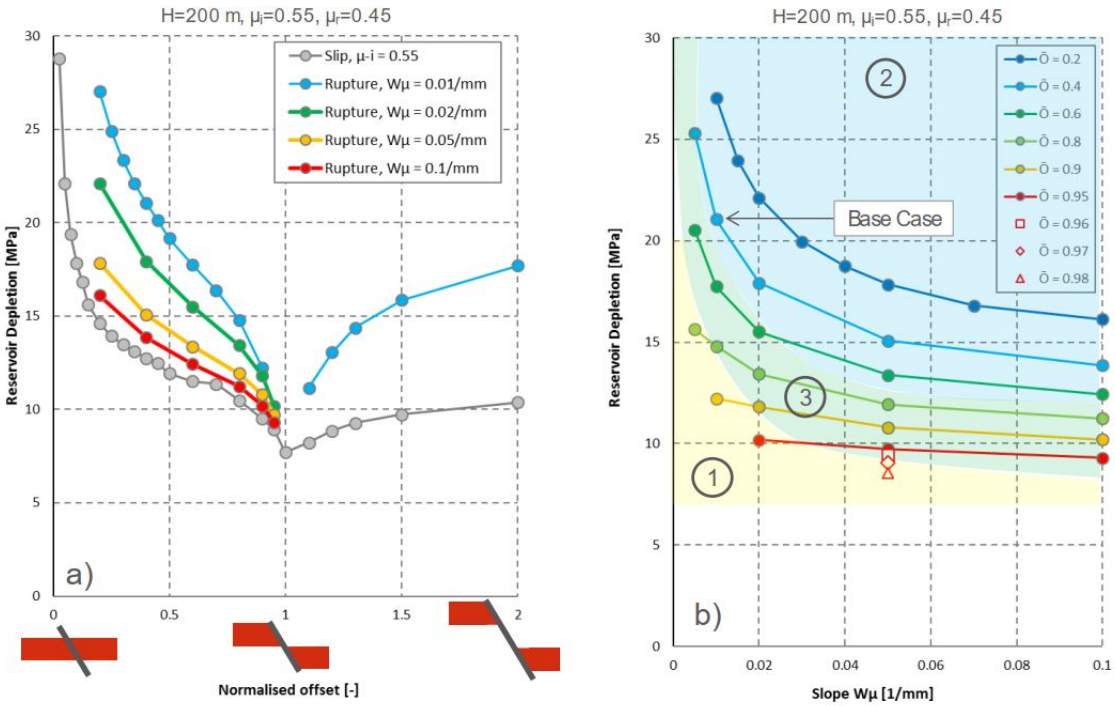

(a) Reservoir depletion versus normalised offset effect on normalised offset

(b) Reservoir depletion versus normalised offset effect on W_μ

Figure 17: Reservoir depletion versus normalised offset (Van den Bogert, 2018)

4.2 Salt impact on stress state

The presence of the viscoelastic Zechstein salt formation can have a dual impact on in situ stress conditions. First, the reservoir rock experiences higher horizontal stresses due to the high horizontal stresses in the salt, which results in a very high effective stress ratio (Muntendam-Bos, 2021). In addition, high horizontal stresses may cause vertical fault intrusion and enlargement, greatly reducing the horizontal stresses in the fault. As a result, salt may intrude locally downward along the fault zone (Roest & Kuilman, 1994, Ketterman et al. 2017). After salt intrudes a fault, the high horizontal stress in the salt amplifies fault dilation and can further reduce horizontal stresses in the fault significantly (Roest & Kuilman, 1994; Jackson & Hudec, 2016; Orlic & Wassing, 2013). Due to salt's poor frictional strength, its presence on a slip surface will weaken faults and make it easier to reactivate. Instead of fault displacement caused by large-scale seismic slip, weak materials like salt operate as a natural fault lubricant, encouraging fault creep followed by micro-earthquakes (Moore & Rymer, 2007; Van der Pluijm, 2011). Furthermore, the viscous nature of the salt prevents stress from accumulating on a fault adjacent to it.

To further understand the effect of the salt, the findings of Leltz (2022) will be discussed, who investigated with numerical models how viscous and isotropic salt influences faults with different offsets. Figure 18 displays the models that he created with Plaxis, which is a software that can be used to investigate the stress system surrounding a fault. The models include the following formations from top to bottom: Zechtstein rocksalt, Zechstein anhydrite/-carbonate, Ten Boer, Slochteren and Carboniferous. The difference between the models is that in model C, the salt is located next to the reservoir along the fault, but it is not in model B. Moreover, it is critical to realize that the reservoir rock used in the study of Leltz is the Rotliegend, which includes the Slochteren formation. Hence, there may be differences in reservoir properties including depth, thickness and friction-coefficient, which may have an impact on the influence of salt.

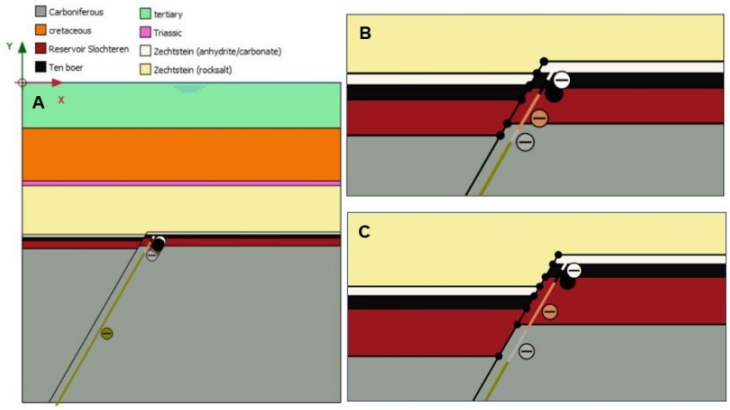

Figure 18: Geological layers of model 1(=B) and 2(=C) (Leltz, 2022)

The presence of salt in the fault raises reservoir stresses. Moreover, the effect of salt on stresses in the fault is greater with larger offsets. When the viscous salt is adjacent to the reservoir, it affects the horizontal stresses and in a smaller way the effective vertical stresses. The presence of salt has relatively small influence on the effective normal stress acting on the fault. The potential of slip occurrence is greater in the fault at reservoir level in the absence of salt and greater at reservoir boundaries in the presence of salt (Leltz, 2022).

Leltz analyzed two cases with and without the presence of salt, for both cases the shear capacity utilization (SCU) was determined (Muntendam-Bos, 2021), which is described in equation 17, where τ is the shear stress and σ_n' is the normal effective stress, μ is the coefficient of friction and C is the coefficient of cohesion and C is presumed to be 0. The stress data is derived from the results of the Plaxis models. If SCU is more than one, failure conditions have been met and slip can occur along the fault. Potential seismic activities can thus be predicted by knowing the SCU along the fault. Based on the results the section along which slip can happen is significantly larger in the case without salt.

$$SCU = \frac{\tau}{C + \sigma_n \mu} \tag{17}$$

Next a new parameter will be introduced, which is called the J ratio. This parameter provides information on the distance between the top of the reservoir and the viscous halite salt and hence whether or not the fault may be affected by the influence of the viscous salt as is previously explained in this section. The J ratio is described by equation 18 and it is a dimensionless ratio that sums the thicknesses of Ten Boer and Carbonates/anhydrites and divides them by the reservoir thickness.

$$J\ ratio = \frac{Ten\ Boer\ +\ Carbonates/Anhydrite\ thickness}{Reservoir\ thickness} \tag{18}$$

All of these thicknesses are known for the gas fields and are sourced from NLOG. This ratio was determined for each field and the results are displayed in the form of a histogram, see Appendix E. A J ratio greater than one implies no juxtaposition of the halite salt with the reservoir. For a J ratio smaller than one, the halite salt may have an influence on the stresses, which depends on the relative offset. When J is larger than the relative offset there is no juxtaposition, but there might be a small intrusion of the salt, which could affect the friction of the fault on the top. When J is smaller or equal to the relative offset, salt does affect the stresses as there is juxtaposition of the halite salt and the reservoir layer.

5 Approach

5.1 Association between the gas field and event

Gas fields from five regions were analyzed the North Holland Platform, the Groningen Platform, the Lauwerszee Trough High Pressures, the Frisian Platform and the Lauwerszee Trough, see figures 19 till 23.

Figure 19: Gas fields in NHP region

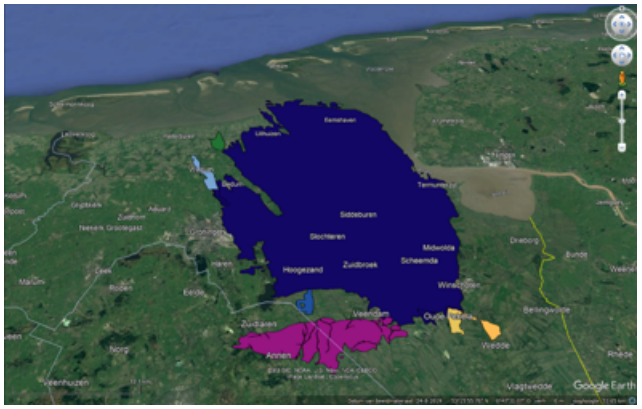

Figure 20: Gas fields in GRO region

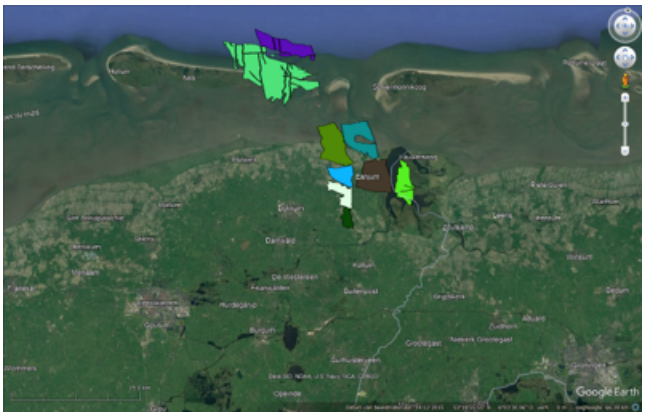

Figure 21: Gas fields in LTHP region

Figure 22: Gas fields in FP region

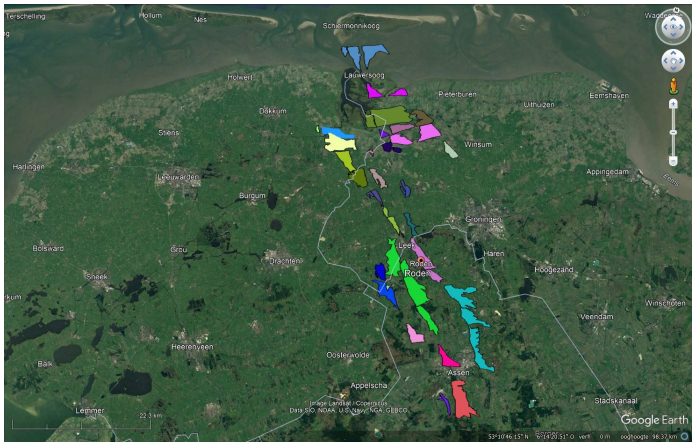

Figure 23: Gas fields in LT region

The gas fields were classified to determine which seismic event could potentially be linked to gas fields. The classification depends upon the location of the event and its radial distance to the field and to nearby fields. In total there are six classes, which are described in table 2. The classification aids in determining which fields will, will not or might become seismically active. The distance measurements were done in Google Earth. A map of events and gas fields were used, respectively sourced from KNMI and NLOG. Figure 24 shows an example of one event and two gas fields. Based on the field classification, gas field 1 falls under class A, because it takes place

within the boundary of the field and no other fields are within 3 km of the event. Gas field 2 falls under class C5, because the field is located within a 5 km radius of the event. Moreover, it is important to know when the production of the gas field started and when the event took place. If the production of a gas field began after the event, it cannot be responsible for that event.

Table 2: Field classification

Class	Description
A	Field definitely seismically active: event(s) recorded within the boundary of the field and no other fields within 3 km of event.
B3	Event(s) recorded within the boundary of the field, but other fields within 3 km of the field
B5	Event(s) recorded within the boundary of the field, but other fields within 5 km of the field
C3	Event recorded near the field (maybe within the boundary of another field), but could be attributed to this field assumming a 3 km location uncertainty
C5	Event recorded near the field (maybe within the boundary of another field), but could be attributed to this field assumming a 5 km location uncertainty
D	No earthquakes within 5 km of the field

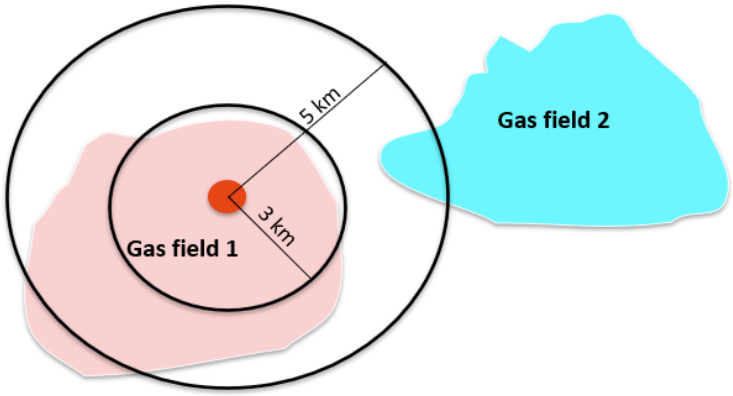

Figure 24: Class determination example with event (red dot) and two gas fields

5.2 Analysis of the most important parameter

Jan-Dirk Jansen and Bernard Meulenbroek created a MATLAB model (version 2.8) that computes and depicts depletion-induced stresses and fault slip along an inclined fault. The model is built around the equations discussed in the previous chapter. The critical slip distance, dip angle, dynamic friction coefficient, Poisson's ratio, porosity, reservoir thickness, shear modulus static friction coefficient, and stress ratio are all subjected to a sensitivity analysis on their impact on the pressure at which seismicity would occur. These parameters are varied whilst the others are kept constant. Ranges of the parameters are based on the most realistic ranges, see table 3. Then for all parameters the range has 10 values. Each parameter has a fixed step size. Table 5 shows the input and output for the porosity parameter. The inputs are the porosity and relative offsets and the output are the pressures. Some of these parameters are reservoir characteristics that are predefined. The sensitivity of these parameters is still examined in order to understand the influence of their uncertainties on the results.

Table 3: Base of parameters

Parameter	Range	Constant
Stress ratio (-)	0.30-0.90	0.60
Reservoir thickness (m)	25-250	100
Critical slip weakening distance (-)	0.001-0.010	0.005
Dynamic friction coefficient (-)	0.25-0.55	0.30
Static friction coefficient (-)	0.50-0.70	0.60
Fault dip (°)	40-90	65
Poisson's ratio (-)	0.10-0.30	0.20
Porosity (-)	0.05-0.35	0.20
Shear modulus (GPa)	6-10	13

6 Sensitivity analysis

The goal of the sensitivity analysis is to define the most sensitive parameters that can be further examined to help determine a regional threshold at which seismicity occurs. This was done with the semi-analytical model, where the inputs are the parameter values and relative fault offset and the output is the pressure depletion at which seismicity occurs. The sensitivity was done on nine parameters, namely the critical slip weakening distance, dip angle, dynamic friction coefficient, Poisson's ratio, porosity, reservoir thickness, shear modulus, static friction coefficient and stress ratio. Each parameter has a realistic range that is based on data from NLOG. Whilst analyzing the range of one parameter, the rest of the parameters are kept constant at a generic average value based on the range. All parameters have a range of 10 values with equal step sizes. The relative fault offset was analyzed for a range from 0.05-0.95 with a step size of 0.5. The relative fault offset is an important characteristic, because gas fields with larger fault offsets are more likely to become seismic at an earlier stage in comparison to faults with a smaller relative offset.

The results are given in figures 25 till 33. The graphs show on the y-axis the pressure depletion at which failure occurs and on the x-axis the normalised fault offset. Furthermore, in the graph the different lines represent the range in the analysed parameter. The general trend is that with larger parameter values for a constant normalised offset the absolute pressure depletion at which seismicity occurs increases. Moreover, all graphs have a nonlinear relationship with a decreasing trend.

6.1 Sensitivity results

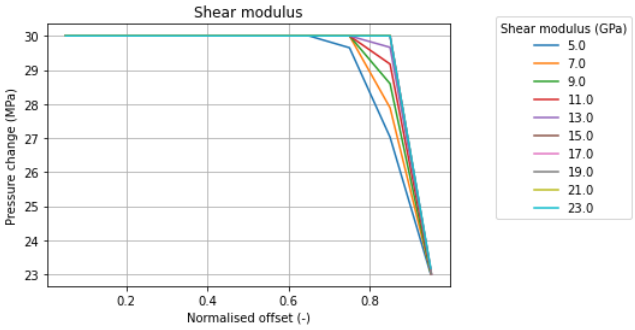

Figure 25: Shear modulus sensitivity

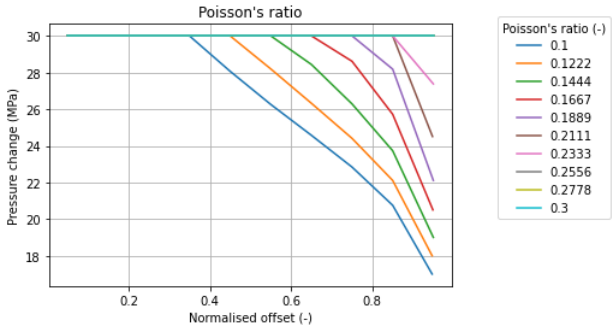

Figure 26: Poisson's ratio sensitivity

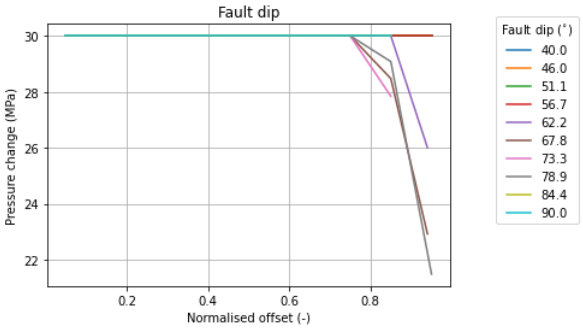

Figure 27: Fault dip angle sensitivity

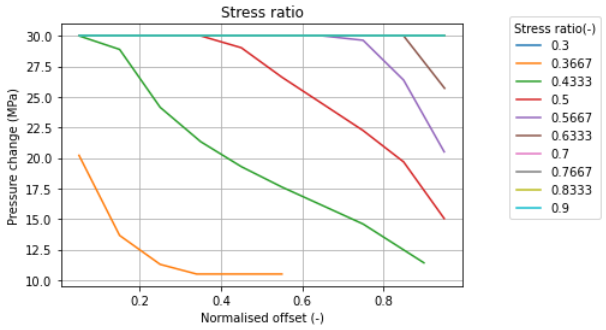

Figure 28: Stress ratio sensitivity

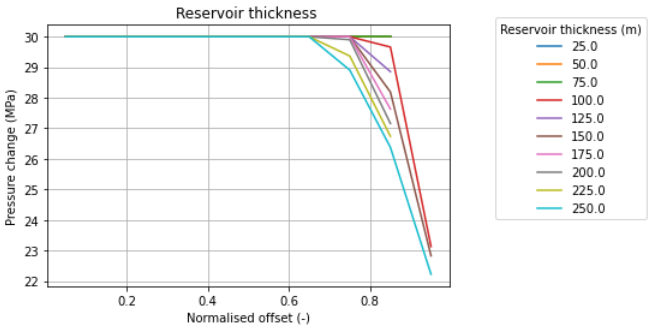

Figure 29: Reservoir thickness sensitivity

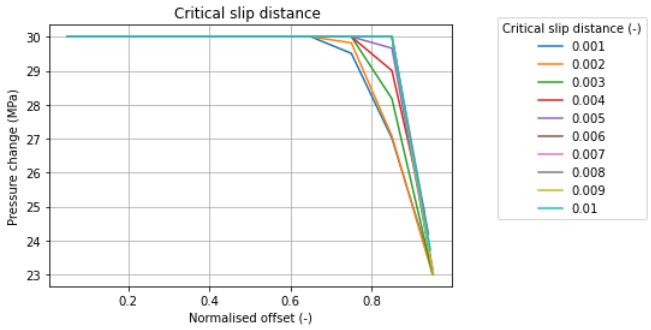

Figure 30: Critical slip distance

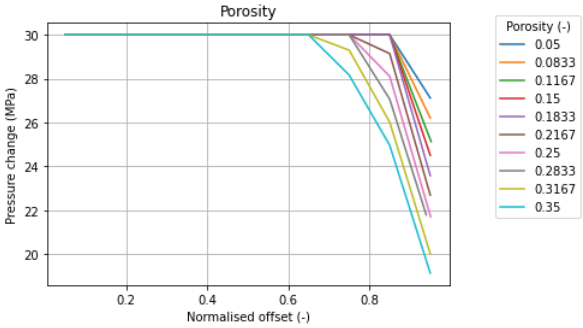

Figure 31: Porosity sensitivity

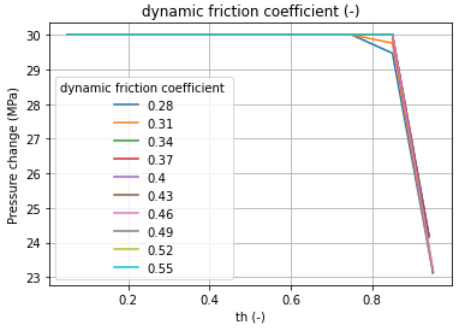

Figure 32: Static friction coefficient sensitivity

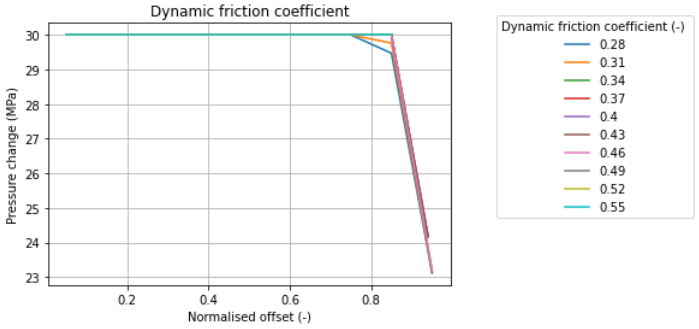

Figure 33: Dynamic friction coefficient sensitivity

6.2 Sensitivity discussion

6.2.1 Shear modulus

The ratio of shear stress to shear strain is known as the shear modulus. This elastic constant describes the shear stiffness. A higher shear modulus value means more force is required to cause deformation. So rocks with smaller shear moduli are more likely to slip. An example of how to read the data will now be given for a fixed normalised offset of about 0.85. For the highest value of 23 GPa, the pressure depletion is smaller (27 MPa), and for the lowest value (5 GPa), the pressure drop is slightly larger, at around 30 MPa. The required depletion pressure drops dramatically around a relative offset of 0.75. The decline is steeper for larger shear moduli. In brief, the lower shear modulus requires less depletion pressure to reach induced seismicity.

6.2.2 Poisson's ratio

The lateral over vertical strain ratio is known as the Poisson's ratio. This parameter, which is also an elastic constant, describes how much a rock expands when it is vertically compressed. In normal faulting there is more vertical than lateral strain. Therefore, smaller values are more likely to fail in an extensional setting. According to the results the relative offset at which the pressure depletion starts to become less than total depletion for the Poisson's ratio ranges from approximately 0.35 to 0.95. With larger Poisson's ratios, the activation of a fault with a lower normalised offset becomes more feasible. In general, as the relative offset increases, the required depletion pressure decreases slightly. Larger Poisson ratio's can fail at smaller relative offsets, whereas smaller Poisson ratio's can only fail at very high offsets. The Poisson's ratio is not seen as crucial because it is related to the compaction coefficient, which is a constant reservoir characteristic.

6.2.3 Reservoir thickness

The reservoir thickness corresponds to the vertical thickness, which roughly represents the average across the entire gas field. Based on the results the depletion pressure is slightly higher in the thinner reservoir. So thicker reservoirs have a higher chance of slipping. The thickness has a relative offset range from 0.65-0.95. The data is not complete for all offsets due to model instabilities. Thicker reservoirs need smaller normalised offset to become seismic. Similar to the shear modulus the required depletion pressure drops dramatically. The decline is faster for thinner reservoirs. Some graphs of the reservoir thickness are missing due to model instabilities, but the parameter has a consistent trend overall.

6.2.4 Fault dip angle

In an extensional setting a fault system is least stable with a 60 degree dip angle. The graphs for the 67.8 and 78.9 degrees intersect at about 25 MPa, which is a unique feature most likely caused by instability in the model. Some graphs in the results are missing, which is also due to instabilities in the model. The fault dip results appear to be too unstable for further analysis.

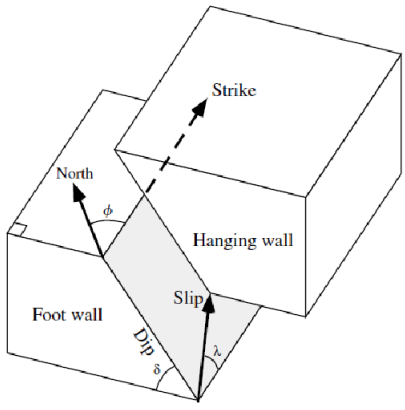

Figure 34: Fault dip (Matrullo, 2012)

6.2.5 Stress ratio

Stress ratio is calculated by dividing initial horizontal effective stress by initial vertical effective stress. The dominant force in extensional conditions for faulting is vertical. Therefore, fault slipping will result more easily from lower stress ratios. The stress ratio includes the whole range of possible relative offsets as can be seen in figure 28. Smaller stress ratios exhibit an exponential decay shape. When the ratio is increased, it becomes somewhat linear, and at higher ratios, it is the inverse of the exponential decay. As a result, the relationship between reservoir depletion and relative offset is also affected by the magnitude of the stress ratio. In general, larger K0's require more depletion to reach seismicity at a fixed offset. Reservoirs with a lower K0 will fail at lower offsets, whereas reservoirs with higher stress ratios require larger offsets.

6.2.6 Critical slip distance

The total slip as the stress decreases to the level of a steady-state friction is known as the critical slip distance (D_c). When D_c is small, the stress on the fault can change dramatically, but as it increases, the change becomes more moderate. Clearly, an abrupt decrease in stress over a short period of time causes high slip rates (Sainoki & Mitri, 2015). This implies that a lower D_c is more likely to cause seismicity, which is in line with the results in figure 30. The required depletion pressure drops dramatically, this time around a relative offset of 0.65. For larger D_c, the decline is faster. At lower pressure depletion levels, smaller critical slip distances fail faster than larger distances. As discussed in the previous chapter, the critical slip weakening distance is critical. The changes with increasing D_c are not uniform, which is striking. The range over which it varies in terms of depletion and normalised offset are relatively small.

6.2.7 Porosity

The porosity is calculated as the void volume divided by the total volume. Higher porosity rocks are less rigid and therefore more prone to slipping. The rate of fracture development is also higher in a more porous rock (McBeck et al., 2019). Based on figure 31 the offset range is approximately 0.65-0.95. In this case, reservoir depletion decreases more gradually with larger offsets. For a fixed offset, the more porous rocks fail at lower reservoir depletions. Meanwhile, faults with smaller offset can only cause failure in less porous rocks. The effect of higher porosity being weaker is reflected in the compaction coefficient.

6.2.8 Dynamic friction coefficient

The dynamic friction coefficient (DFC) is the force exerted by two objects against one another when one of the objects is moving. In the case of this study it can be described as the friction on the fault as seismic slip occurs on the fault. Low values indicate little friction and increase the slipping risk. For all dynamic friction coefficients, the pressure depletion that causes fault slip drops in the same manner. An increase in dynamic friction coefficient does not affect the likelihood of failure. The DFC has little variation for the pressure depletion in the range of the parameter and it has limited results due to model instabilities.

6.2.9 Static friction coefficient

The friction force between two objects when neither is moving is known as the static friction coefficient (SFC). Low values indicate little friction and increase the slipping risk. According to the findings in figure 33 at a fixed offset, failure is more likely with lower SFC values. While higher SFC reservoirs need higher reservoir depletions. Furthermore, some of the data is missing as a result of program instabilities.

6.3 Sensitivity conclusion

Later on, in the analysis of the most sensitive parameter, specific gas field parameter inputs will be used, which are the compaction coefficient, initial pressure, reservoir depth and thickness. The compaction coefficient is related to the Poisson's ratio. So, the compaction coefficient and reservoir thickness are not appropriate sensitive parameters, because they are predetermined. The results show that the stress ratio and Poisson's ratio have the most variability out of all the parameters. The Poisson's ratio is related to the compaction coefficient, which is a reservoir parameter that will later on be given as an input in the model. Hence, it is not an appropriate sensitive parameter as it was already predefined. Hence, the stress ratio is the most sensitive parameter.

6.4 Most sensitive parameter

After obtaining the most sensitive parameter, the next step is to determine for this parameter the range that indicates the occurrence of seismicity. Moreover, the relation between the two important parameters is also discussed.

Since the stress ratio is the most critical parameter it is plotted without the influence of the other parameters by keeping them constant. These constants are based on the most realistic values of the subsurface. The dimensionless critical slip weakening distance was set at 0.001, so the minimum pressure at which failure would occur is conservative. This is done for each gas field, which has its own reservoir characteristics, reservoir thickness, compaction coefficient, reservoir depth, minimum and maximum normalised offset and initial pressure. If needed the initial pressure is adjusted by taking off the substantial overpressure. The output is the pressure in MPa at which seismicity would occur. These calculations were done for each gas field. An example of the Groet gas field is shown in table 6 in Appendix B. Based on this table, the stress ratio at which seismicity would occur with the smallest offset in this situation can be determined. The stress ratio's at which the depletion pressure and the first seismic event pressure are reached are required. The depletion pressure is the total depletion pressure and the first event pressure is the depletion pressure at the time of the first seismic event.

The ranges of the K0 at the total depletion and the first event were then determined using this data. The values closest to the needed pressure were used for both the minimum and maximum normalised offset. This was done to derive exact values with a one decimal accuracy as well as values with a step size of 2/3. The exact results and the input data for NHP which includes Groet is shown in Appendix 7. The exact results are shown as bar plots in the results chapter. The bottom of the K0 bar plots responds with the minimum relative offset and top with the maximum relative offset. Faults with higher relative offsets become active sooner than faults with lower offsets (Van Thienen-Visser et al., 2018). To activate both simultaneously, the initial stress ratio for the higher offset faults must be greater and therefore further away from activation, than the stress ratio for the smaller offset faults. Hence, the initial stress situation must be closer to failure. Afterwards, the fields were analyzed in order to determine a regional stress ratio. Outliers were then investigated and re-evaluated using geological and geomechanical information. Moreover, the LTHP and LT region are calculated without the influence of overpressure. To accomplish this, the initial pressure must be adjusted by substracting the overpressure. Since there are high overpressures in these regions.

6.5 Trade-off between the stress ratio and critical slip distance

The stress ratio was compared to the critical slip distance, to give an example of the relationship between parameters. Since minor changes in these parameters have a large impact on when they will become seismic at various offsets and depletion pressures, their relationship is depicted in interactive 3D plots. For each field the K0 was plotted against the Dc and on the y axis the depletion pressure. Including a surface representing the pressure at the first seismic event, or the total depletion if no seismicity has occurred. The range for the K0 is [0.3, 0.3667, 0.4333, 0.5, 0.5667, 0.6333, 0.7, 0.7667, 0.8333, 0.9] and for the Dc is [0.001, 0.002, 0.003, 0.004, 0.005, 0.006, 0.007, 0.008, 0.009, 0.01]. These are the same ranges that were used previously. The K0 has a step size of 2/3 and Dc of 1/1000. The other important parameters were kept constant. The minimum and maximum normalised relative offset were used for these plots. It is possible to put it in a 3D representation in Jupyter notebook. The code for this is shown in the Appendix A.

7 Results

7.1 Field classification

The field classification indicates the likelihood of the gas field causing a seismic event. The classification is used for all of the minor gas fields in the Netherlands. There are six classes in total: A, B3, B5, C3, C5, and D. The events associated with the field are displayed in the last column. The event's date, name, and magnitude (M) are provided. Emmen, Roswinkel, Vries, Eleveld, and Annerveen all have a lot of events, more than five, thus not all of them are mentioned.

Table 4: Field classification of five regions *(T0prod:starting time of gas production)*

Region NHP				
Field	**T0prod (YYYY-MM-DD)**	**Class**	**Oldest event (date (YYYY-MM-DD), name, magnitude)**	**All events (date (YYYY-MM-DD), name, magnitude)**
Bergen ROSL	1978-10-13	C3	2001-10-10, Schoorl, M=2.7	2001-10-10, Schoorl, M=2.7; 2012-03-16, Noordzee (near Schoorl), M=1.0; 2012-04-18, Noordzee (near Schoorl), M=1.8
Bergermeer	1972-09-01	A	1994-08-06, Bergen, M=3.0	1994-09-21, Bergen, M=3.2; 1994-08-06, Bergen, M=3.0; 2001-09-10, Bergen, M=3.2; 2001-09-09, Bergen, M=3.5
Groet	1974-01-01	C3	2001-10-10, Schoorl, M=2.7	2001-10-10, Schoorl, M=2.7; 2012-03-16, Noordzee (near Schoorl), M=1.0; 2012-04-18, Noordzee (near Schoorl), M=1.8
Groet-Oost	2006-02-01	C5	2012-03-16, Noordzee (near Schoorl)	2012-03-16, Noordzee (near Schoorl), M=1.0; 2012-04-18, Noordzee (near Schoorl), M=1.8
Middelie ROSL	1975-08-01	C3	1989-12-01, Kwadijk, M=2.7	1989-12-01, Kwadijk, M=2.7; 2018-06-04, Warder, M=2.5
Middenmeer	1977-07-01	D	x	x
Rustenburg	2009-09-01	D	x	x
Schermer (rot)	1979-09-01	D	x	x
Westbeemster	2007-11-01	D	x	x

Region LTHP				
Field	**T0prod (YYYY-MM-DD)**	**Class**	**Oldest event (date (YYYY-MM-DD), name, magnitude)**	**All events (date (YYYY-MM-DD), name, magnitude)**
Ameland-Oost	1986-01-01	C3	2005-03-21, Buren, M=1.8	2005-03-21, Buren, M=1.8; 2013-08-09, Waddenzee (near Buren), M=1.8
Ameland-Westgat	1993-01-01	D	x	x
Anjum	1997-08-01	C3	2005-05-28, Morra, M=1.4	2005-05-28, Morra, M=1.4
Ezumazijl	1999-02-01	D	x	x
Metslawier	1997-12-01	B3	2005-05-28, Morra, M=1.4	2005-05-28, Morra, M=1.4
Metslawier-Zuid	2012-05-01	C5	2012-10-16, Kollum, M=1.1	2012-10-16, Kollum, M=1.1; 2016-10-30, Kollum, M=1.5
Moddergat	2007-02-05	D	x	x
Nes	2007-02-01	D	x	x
Oostrum	2002-10-01	C3	2012-10-16, Kollum, M=1.1	2012-10-16, Kollum, M=1.1; 2016-10-30, Kollum, M=1.5

Region GRO				
Field	**T0prod (YYYY-MM-DD)**	**Class**	**Oldest event (date (YYYY-MM-DD), name, magnitude)**	**All events (date (YYYY-MM-DD), name, magnitude)**
Annerveen	1973-01-01	A	1994-08-16, Anloo, M=2.3	Etc.

Bedum	1985-11-01	B3	2008-04-15, Wetsinge, M=0.9	2008-04-15, Wetsinge, M=0.9; 2013-07-08, Wetsinge, M=1.6; 2016-05-11, Bedum, M=0.4; 2018-12-19, Bedum, M=1.0; 2018-09-18, Bedum, M=0.7; 2019-06-14, Bedum, M=0.9; 2021-03-09, Wetsinge, M=0.7;
Blijham	1984-01-01	C5	2012-01-27, Oude Pekela, M=1.6	2012-01-27, Oude Pekela, M=1.6
Groningen	1963-01-01	A	Etc.	Etc.
Kiel-Windeweer	2003-11-01	C3	2006-03-04, Hoogezand, M=1.8	Etc.
Oude Pekela	1995-01-01	C3	2012-01-27, Oude Pekela, M=1.6	2012-01-27, Oude Pekela, M=1.6
Warffum	1986-10-01	B3	2006-04-23, Warffum, M=1.1	2006-04-23, Warffum, M=1.1
Zuidwending-Oost	2006-07-01	C3	2011-05-02, Meeden, M=1.2	2011-05-02, Meeden, M=1.2; 2020-08-21, Veendam, M=0.7; 2012-01-27, Oude Pekela, M=1.6; 2018-03-08, Veendam, M=0.7

Region FP

Field	T0prod (YYYY-MM-DD)	Class	Oldest event (date (YYYY-MM-DD), name, magnitude)	All events (date (YYYY-MM-DD), name, magnitude)
Appelscha	1999-11-01	A	2003-01-13, Ravenswoud, M=1.7	2003-01-13, Ravenswoud, M=1.7; 2003-06-16, Ravenswoud, M=2.3
Blija-Ferwerderadeel	1985-01-01	D	x	x
Blija-Zuid	2012-09-01	D	x	x
Blija-Zuidoost	2001-01-01	D	x	x
De Hoeve (rotliegend)	2012-04-01	D	x	x
Diever	2015-10-01	D	x	x
Eernewoude	2012-11-27	D	x	x
Eesveen	2015-04-01	D	x	x
Harkema	2010-05-01	D	x	x
Marum	1978-01-01	B3	2020-02-22, Opende, M=1.4	2020-02-22, Opende, M=1.4
Middelburen	1980-01-01	D	x	x
Opende-Oost	1993-01-01	C5	2020-02-22, Opende, M=1.4	2020-02-22, Opende, M=1.4
Suawoude	1984-01-01	D	x	x
Surhuisterveen	2008-09-01	C5	2020-02-22, Opende, M=1.4	2020-02-22, Opende, M=1.4
Tietjerksteradeel ROSL	1974-01-01	C5	2003-02-14, Boelenslaan, M=1.8	2003-02-14, Boelenslaan, M=1.8
Ureterp	1978-01-01	C3	1999-04-22, Ureterp, M=1.0	1999-04-22, Ureterp, M=1.0; 2003-02-14, Boelenslaan, M=1.8; 2020-02-22, Opende, M=1.4

Region LT

Field	T0prod (YYYY-MM-DD)	Class	Oldest event (date (YYYY-MM-DD), name, magnitude)	All events (date (YYYY-MM-DD), name, magnitude)
Assen	2007-07-01	C5	2009-11-19, Assen, M=0.9	2009-11-19, Assen, M=0.9; 2011-09-22, Assen, M=0.9; 2014-02-05, Assen, M=2.0
Boerakker	1998-07-01	C3	2012-07-10, Lettelbert, M=0.9	2012-07-10, Lettelbert, M=0.9; 2019-08-04, Boerakker, M=0.7
Een	2005-05-01	D	x	x

Eleveld	1975-01-01	B3	26-12-1986, Assen, M=2,8	26-12-1986, Assen, M=2,8; 14-12-1987, Hooghalen, M=2.5; 1991-08-08, Assen, M=2.7; Etc.
Engwierum	2002-10-01	C3	2012-10-16, Kollum, M=1.1	2012-10-16, Kollum, M=1.1; 2016-10-30, Kollum, M=1.5
Faan	2009-02-01	C5	2015-03-01, Kommerzijl, M=1.5	2015-03-01, Kommerzijl, M=1.5
Feerwerd	2000-10-01	C3	2004-05-24, Wetsinge, M=1.4	2004-05-24, Wetsinge, M=1.4; 2004-05-29, Winsum, M=0.8; 2004-05-31, Winsum, M=0.3; 2006-12-25, Leens, M=1.3
Grootegast	1979-01-01	C3	1997-03-02, Pieterzijl, M=1.3	1997-03-02, Pieterzijl, M=1.3
Houwerzijl	2000-06-01	C3	2006-12-25, Leens, M=1.3	2006-12-25, Leens, M=1.3; 2013-01-09, Houwerzijl, M=1.0; 2015-03-01, Houwerzijl, M=1.4; 2015-03-01, Houwerzijl, M=1.4; 2018-04-07, Lauwerzijl, M=1.7; 2018-04-07, Kommerzijl, M=1.0; 2020-01-23, Kommerzijl, M=0.4; 2021-02-28, Munnekezijl, M=1.3
Kollum	2002-11-01	B3	2012-10-16, Kollum, M=1.1	2012-10-16, Kollum, M=1.1; 2016-10-30, Kollum, M=1.5
Kollumerland	1989-01-01	C5	1997-03-02, Pieterzijl, M=1.3	1997-03-02, Pieterzijl, M=1.3; 2012-10-16, Kollum, M=1.1; 2016-10-30, Kollum, M=1.5
Kollum-Noord	2001-10-01	C3	2015-03-01, Kommerzijl, M=1.5	2015-03-01, Kommerzijl, M=1.5; 2012-10-16, Kollum, M=1.1; 2016-10-30, Kollum, M=1.5
Kommerzijl	2001-02-01	B3	2018-04-07, Kommerzijl, M=1.0	2018-04-07, Kommerzijl, M=1.0; 2020-01-23, Kommerzijl, M=0.4
Lauwersoog Oost	2008-10-01	D	x	x
Lauwersoog West	2008-10-01	D	x	x
Lauwersoog Centraal	2008-10-01	D	x	x
Leens	2003-01-01	C3	2006-12-25, Leens, M=1.3	2006-12-25, Leens, M=1.3; 2015-03-01, Houwerzijl, M=1.4
Molenpolder	2001-10-01	C5	2015-03-01, Kommerzijl, M=1.5	2015-03-01, Kommerzijl, M=1.5
Munnekezijl dev 1	1995-02-01	B3	2021-02-28, Munnekezijl, M=1.3	2021-02-28, Munnekezijl, M=1.3
Norg	1983-01-01	C3	1993-03-05, Langelo, M=1.5	1993-03-05, Langelo, M=1.5; 1995-06-03, Tolbert, M=0.9; 1996-09-02, Roden, M=2.1; 1996-11-30, Nietap, M=1.0; 1999-06-07, Steenbergen, M=1.1; 2019-08-04, Boerakker, M=0.7
Norg-Zuid	1999-09-01	D	x	x
Pasop	1997-08-01	C3	2015-03-01, Houwerzijl, M=1.4	2012-07-10, Lettelbert, M=0.9
Pieterzijl-Oost	2016-01-01	C3	2020-01-23, Kommerzijl, M=0.4	2020-01-23, Kommerzijl, M=0.4

Roden	1976-01-01	B3	1995-06-03, Tolbert, M=0.9;	1995-06-03, Tolbert, M=0.9; 1995-10-18, Peize, M=1.3; 1996-09-02, Roden, M=2.1; 1996-11-30, Nietap, M=1.0; 1996-12-28, Bunne, M=1.8; 1996-12-28, Bunne, M=1.9; 1997-11-03, Donderen, M=1.4; 2002-03-17, Donderen, M=0.4; 2012-07-10, Lettelbert, M=0.9; 2020-09-26, Winde, M=0.9; 2020-09-27, Winde, M=1.8
Saaksum Oost	1999-04-01	B3	2006-12-25, Leens, M=1.3	2006-12-25, Leens, M=1.3
Saaksum West	1999-04-01	B3	2013-01-09, Houwerzijl, M=1.0	2013-01-09, Houwerzijl, M=1.0
Sebaldeburen	1997-07-01	C3	2019-08-04, Boerakker, M=0.7	2019-08-04, Boerakker, M=0.7
Vierhuizen-Oost	2008-06-01	C5	2021-02-28, Munnekezijl, M=1.3	2021-02-28, Munnekezijl, M=1.3
Vries Centraal	1976-01-01	B3	2000-07-10, Vries, M=1.0	2000-07-10, Vries, M=1.0; 2000-07-13, Vries, M=1.1; 2017-10-11, Vries, M=0.7; 2020-07-27, Vries, M=1.0
Vries Noord	1976-01-01	B3	1996-12-28, Bunne, M=1.9; 1996-12-28, Bunne, M=1.8	1996-12-28, Bunne, M=1.9; 1996-12-28, Bunne, M=1.8; 1997-11-03, Donderen, M=1.4; 2002-03-17, Donderen, M=0.4
Vries Zuid	1976-01-01	C3	2002-09-22, Taarlo, M=0.5	2002-09-22, Taarlo, M=0.5; 2007-11-30, Ubbena, M=1.5; 2008-12-24, Vries, M=1.2
Wieringa	2012-11-26	C3	2013-01-09, Houwerzijl, M=1.0	2013-01-09, Houwerzijl, M=1.0; 2018-04-07, Lauwerzijl, M=1.7; 2018-04-07, Kommerzijl, M=1.0; 2020-01-23, Kommerzijl, M=0.4
Witterdiep	2007-06-01	B3	2008-10-26, Hooghalen, M=1.7	2008-10-26, Hooghalen, M=1.7
Zevenhuizen	2008-07-01	D	x	x

7.2 Interactive 3D representation of relation between stress ratio and critical slip distance

The 3D model in figure 40 shows the stress ratio on the x-axis, critical slip distance on the y-axis and pressure change on the z-axis. The interactive model can be displayed in Jupyter Notebook with the code in Appendix A. The graphic shows the combination of two characteristics that allows seismicity to occur, as well as the pressure at which it occurs. The general trend is that seismicity occurs at higher pressures for higher stress ratios, but this is not the case for the critical slip distance. Seismicity can occur across the entire pressure range for all the critical slip values, because the influence is more limited. Small changes in the critical slip distance might generate a significant correlation between the parameters and the pressure depletion, resulting in an incorrect estimate of the stress ratio.

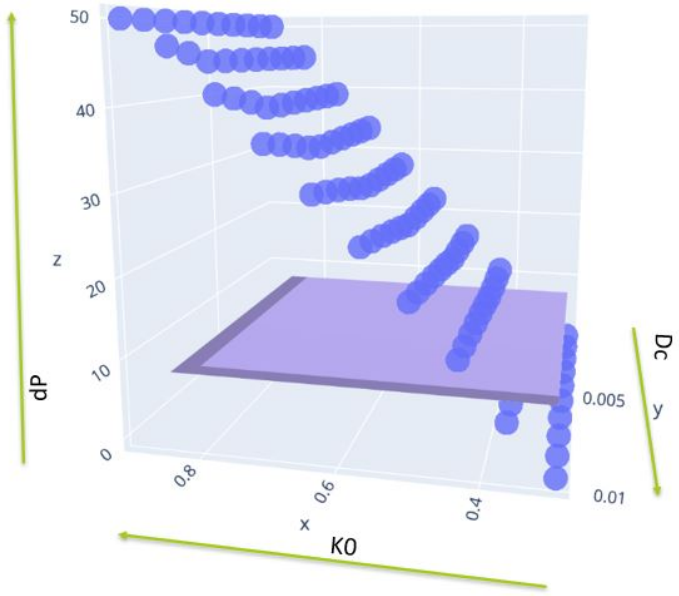

Figure 35: Blija-Zuidoost with maximum offset, dP vs K0 vs Dc

7.3 Stress ratio data

For each of the five regions, the seismicity stress ratio ranges for the gas fields are displayed. The minimum and maximum stress ratios are computed using the minimum and maximum offsets, respectively. The green bars are based on pressure data of the initial seismic event, whereas the blue bars are based on pressure data of the total depletion. Some gas fields have an asterisk next to their name, because they do not have any internal faults and are given dummy data for their fault offsets. The stress ratio ranges for LT and LTHP are also presented without the effect of the overpressure.

7.3.1 North Holland Platform

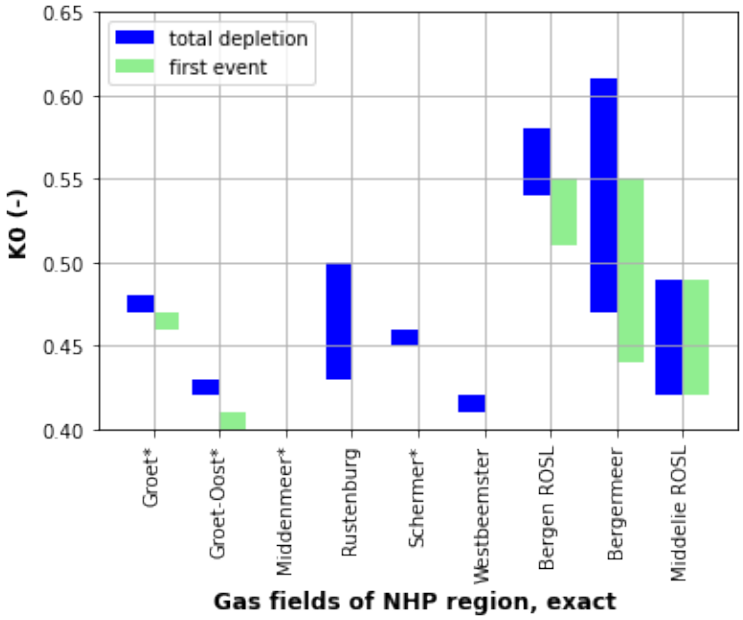

Figure 36: K0 ranges for NHP region

7.3.2 Lauwerszee Trough High Pressures

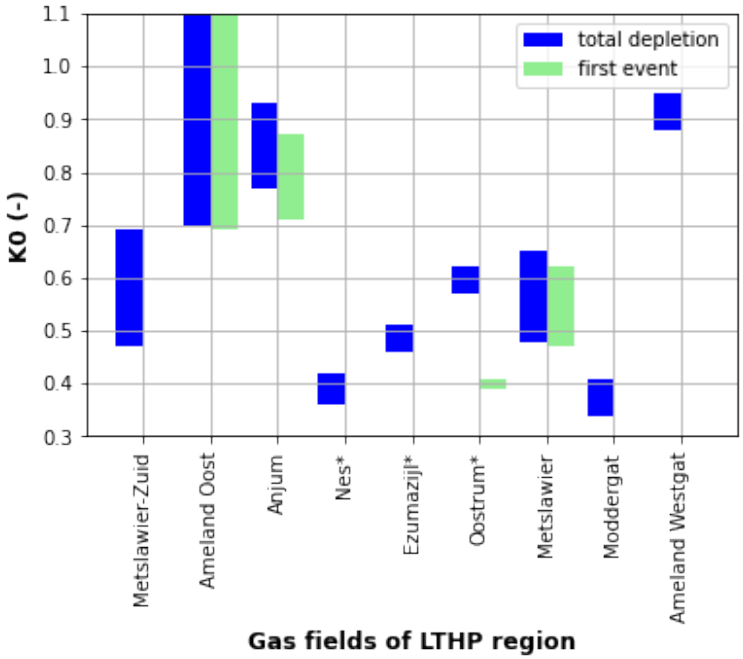

Figure 37: K0 ranges for LTHP region

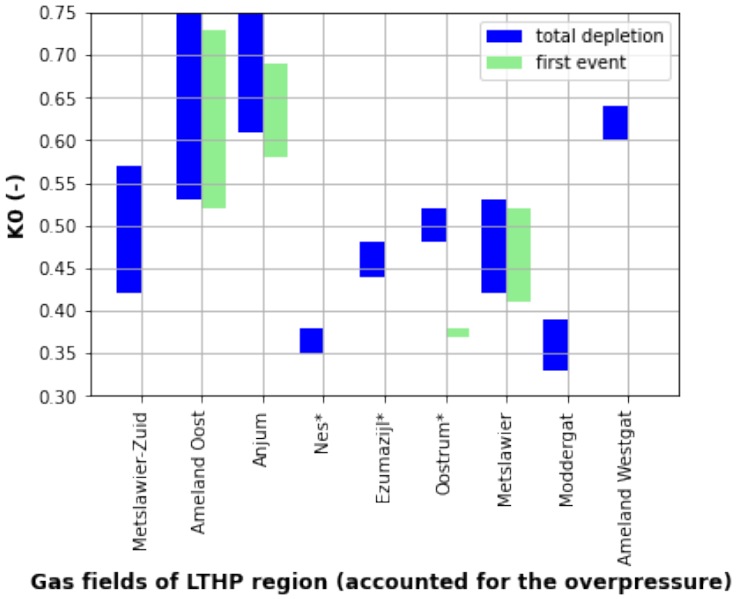

Figure 38: K0 ranges for LTHP region without overpressure

7.3.3 Groningen

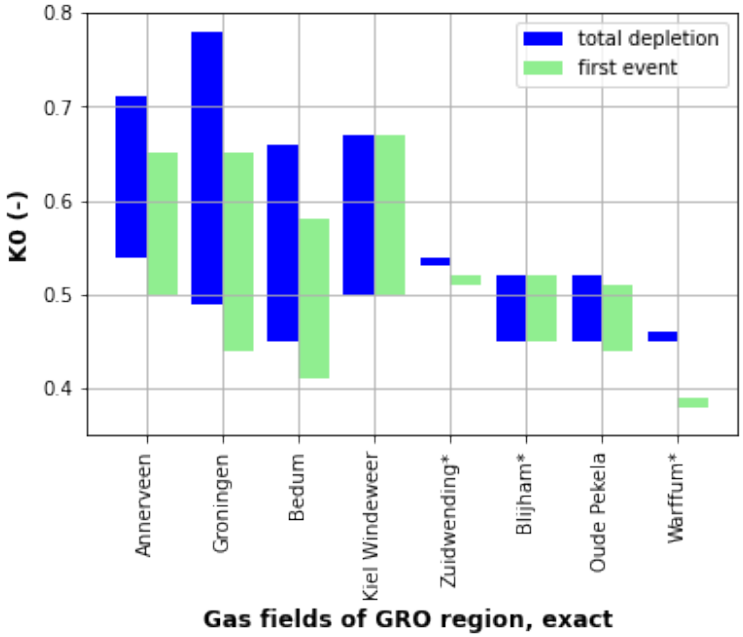

Figure 39: K0 ranges for GRO region

7.3.4 Frisian Platform

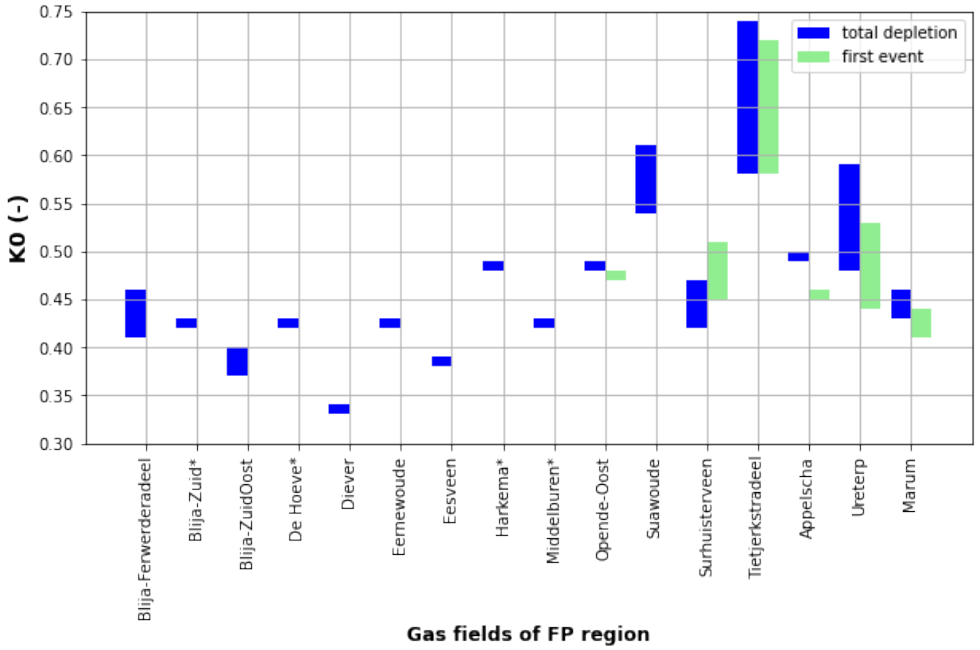

Figure 40: K0 ranges for FP region

7.3.5 Lauwerszee Trough

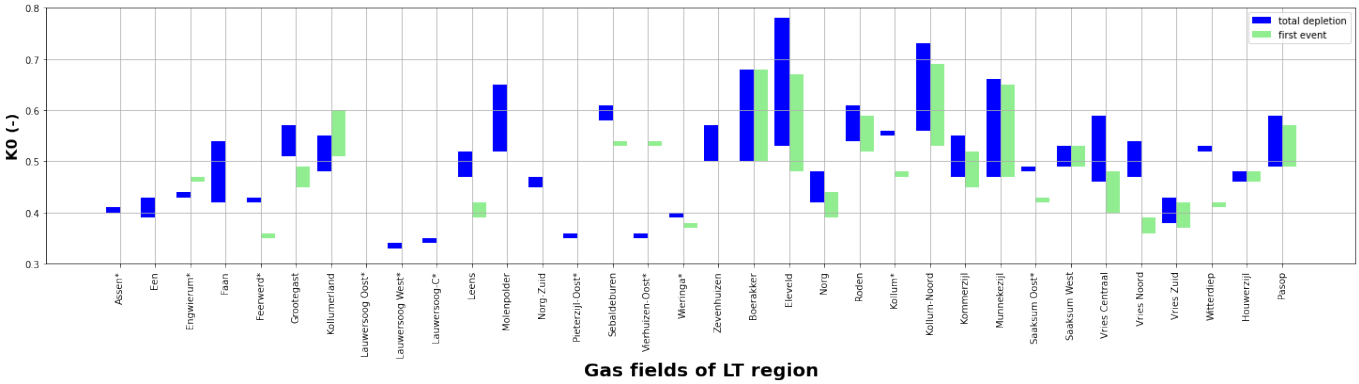

Figure 41: K0 ranges for LT region

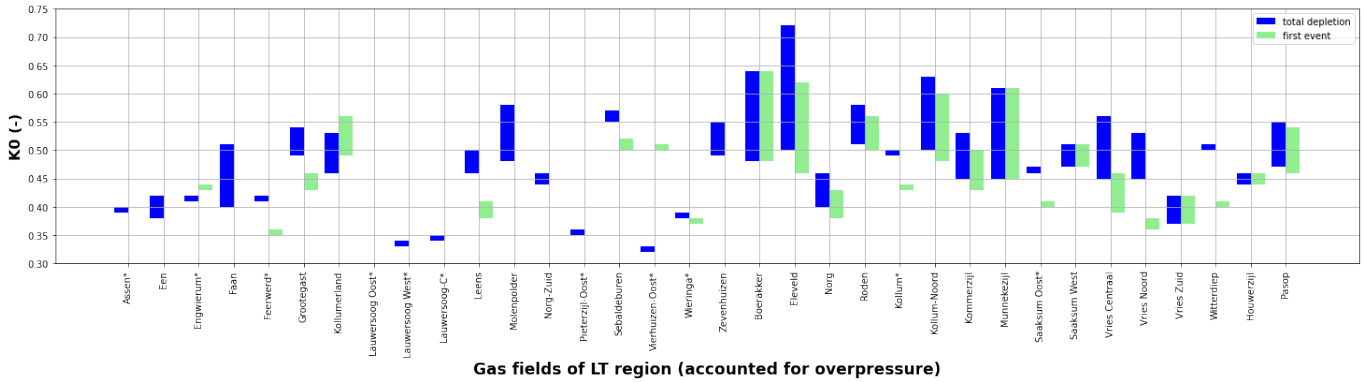

Figure 42: K0 ranges for LT region without overpressure

8 Discussion

8.1 Regional stress ratio

The goal is to determine the regional stress ratio that can explain the (non-)occurrence of seismic activity in all gas fields. In this chapter these stress ratio's are defined based on the results in the previous chapter and discussed. It should be mentioned that some fields only have one fault offset and in order to have a minimum and maximum offset, a minimum fault offset of 10 meters is given, unless the present fault offset is smaller or equal to 10 meters. Furthermore, other fields have no internal offset at all and these are given a maximum artificial offset of 10 meters in order to see how the field would behave if it had an undetected internal offset.

8.1.1 North Holland Platform

The fields that should not become seismically active are Groet-Oost, Rustenburg, Schermer and Westbeemster. All of these have a low stress ratio range except for Rustenburg, which could be due to an overestimation of the maximum fault offset based on figure D.2. Rustenburg is positioned in a tilted and faulted block. So the maximum fault offset is very local. In order to induce seismicity a larger fault area is needed. So the largest offset is possibly not a good indicator of the offset at which seismicity will occur. The smaller offsets do not lead to seismicity. Hence, it is assumed that no seismicity should have been recorded despite the largest offsets being seismically activated. Moreover, Groet has no internal faults and its results are based on synthetic data. Hence, the event is very unlikely to be associated with Groet. The event can also, within my field classification, easily be associated with Bergen which is seismically active and can be explained consistently.

Bergen ROSL and Bergermeer have stress ratio ranges that are relatively high and are assumed to be definitely seismically active. Middelie ROSL has a stress ratio range that is relatively low. For Middelie ROSL the minimum offset of 25 meters does seem reasonable based on the structural map, but there could still be some uncertainties in the structural data. Since 1976 gas is produced from both the Rotliegend sandstone and Zechstein formation. So, it is hard to say in which formation the depletion pressure took place that caused the seismic event. In the Rotliegend formation there is a small fault offset of about 25 meters, based on structural data. The approximate depletion pressure is larger in the wells that produced from the Zechstein formation. Hence, it is assumed that the seismicity occurred due to a fault in the Zechstein formation. The second seismic event is most likely associated with Middelie, so it is most likely a seismic field. These assumptions lead to a regional stress ratio of 0.51, see figure 43.

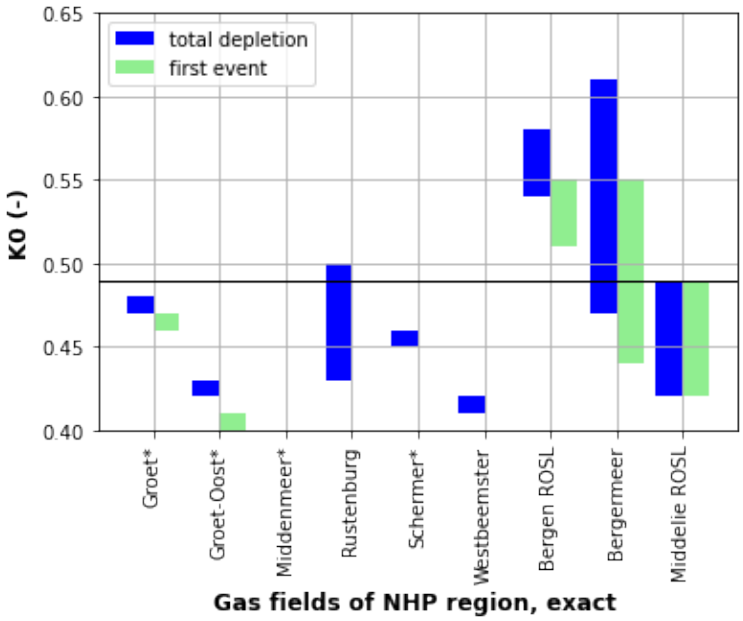

Figure 43: NHP K0 range

8.1.2 Lauwerszee Trough High Pressures Platform

A scenario with and without overpressures was created for LTHP. The stress ratio for Ameland-Oost is no longer more than 1.0 in the absence of overpressures, which is logical as it would otherwise imply that the field should always have been seismically active. The data that accounts for overpressure will be used to determine the regional stress ratio, because it is more realistic.

The fields that should be below the regional stress ratio, as they are all definitely not associated with seismicity, are Metslawier-Zuid, Nes, Ezumazijl, Moddergat and Ameland-Westgat. Ameland-Westgat is a very special case due to its relatively high maximum stress ratio. Oostrum is unlikely to create seismicity, because it lacks internal faults. The event associated with Oostrum can also be linked to Kollum or Kollum-Noord, which explains the low stress ratio range. Hence, Oostrum is assumed to not have induced seismicity. The first seismic event linked to Anjum and Metslawier are the same. Based on the geomechanics, Anjum is more logical to have induced the event given the high stress ratio. Hence, Anjum is very likely to be associated with seismic activity.

So Metslawier is not assumed to be responsible for any seismicity. The event that is associated with Ameland-Oost cannot be linked to any other field, so it must be seismically active. Eventually, a regional stress ratio of 0.69 is chosen, see figure 44.

Only the LTHP region has no juxtaposition with salt, according to the J ratio histograms in Appendix E, since the J ratio is for all fields bigger than one. As a result, its stress state on the fault remains unaffected by salt. However, the stress ratio within the formation is affected by the very thick salt deposits (Verweij et al., 2016).

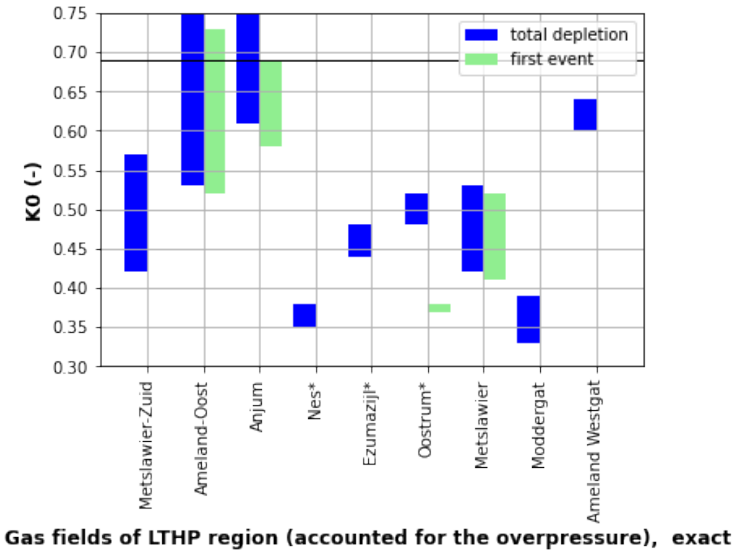

Figure 44: LTHP K0 range

8.1.3 Groningen

Blijham, Oude Pekela, Warffum and Zuidwending have relatively low stress ratio ranges. Blijham, Warffum and Zuidwending contain no internal faults therefore they are unlikely to be seismically active. They were provided with dummy data and should all be positioned below the regional stress ratio. Oude Pekela is classified as a C3 field. The seismic event associated with Oude Pekela could alternatively belong to either Groningen or Zuidwending-Oost. Zuidwending-Oost lacks internal faults, which means it is not a good alternative. Groningen is a good possibility because it also takes place within the boundaries of Groningen. As a result, it is assumed that Oude Pekela was not seismically active and the event is most likely related to Groningen.

Annerveen, Bedum, Groningen and Kiel Windeweer are expected to be above the regional stress ratio, as they are all definitely associated with seismicity and due to their high stress ratio ranges. Annerveen has a complex structural geology, which predominantly includes N-S orientated scissor faults. Furthermore, based on the stress ratio results in figure 45, Kiel Windeweer became active earlier than anticipated compared to the other fields due to the maximum fault offset. Based on the information the regional stress ratio for Groningen is 0.58, see figure 45.

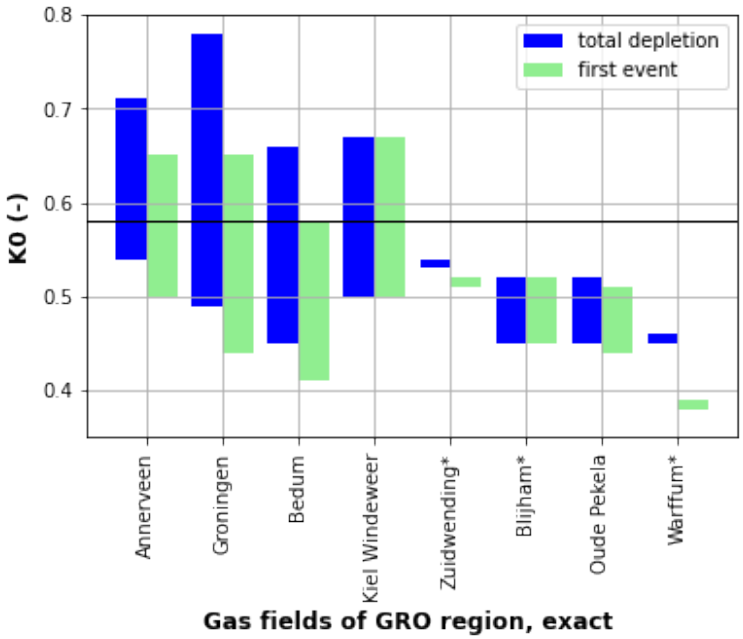

Figure 45: GRO K0 range

8.1.4 Frisian Platform

The gas fields of the FP region can be divided into three smaller areas, namely North, Central and South. In the North area there are three fields: Blija-Ferwerderadeel, Blij-Zuid and Blija-Zuidoost. In the Central area there are eight fields Eernewoude, Harkema, Middelburen, Opende-Oost, Suawoude, Surhuisterveen, Tietjerksteradeel, Ureterp and Marum. In the South area there are four fields which are Appelscha, De Hoeve, Diever and Eesveen.

The fields in the North area are all classified as D fields. Hence, the regional stress ratio can have any value above 0.46.

In the Central area, there are two fields that do not have any internal faults, Harkema and Middelburen. Hence, their stress ratio range is expected to be below the regional stress ratio. Eernewoude is a D field and has a relatively low stress ratio. So it is not expected to be seismically active. The first event of Marum is also linked to Opende-Oost, Surhuisterveen and Ureterp. The event is most likely related to Ureterp. Hence, Marum would not be associated with any seismicity. Suawoude has a relatively high range for the stress ratio from 0.54 - 0.61 and a very minor internal fault with a low offset. If this fault would have been reactivated it would produce small magnitude events, which would be undetected. It can be assumed that Suawoude has been seismically active, but the magnitude of the earthquake was too small to be registered. In the past lower magnitudes could not be registered, due to less accurate tools. The magnitude of an event is also dependent on the fault surface. In the case of relatively small offsets, the slip patches do not come together during the earthquake, so the maximal magnitude is never reached (Van den Bogert, 2018). Suawoude has minimal and maximum relative offsets of about 0.07 and 0.17, which are consistent with the scenario. Figure 47 shows a cross-section of Suawoude. The reservoir is made up of two reservoir blocks, which are separated by an internal fault. The southern block was drilled in 1997 and found undepleted pressures. Besides that, the southern fault between the two blocks is a boundary fault. Tietjerksteradeel has a relatively large stress ratio values. The cause could be the overestimation of the offset, based on the structural map from NLOG from 2010. I suggest that a new structural map with more data would help to obtain a more accurate offset. Opende-Oost, Surhuisterveen and Ureterp are associated with seismic events and have relatively high stress ratio's. Hence, they are expected to be responsible for seismic activity. For the Central area a regional stress ratio of 0.47 is chosen.

Fields in the South area that have not been associated with any seismicity are Eesveen, De Hoeve and Diever. For Appelscha to have become active at the time of the first event, and all other fields in the south to not be activated, a stress ratio of 0.46 is needed, see figure 46.

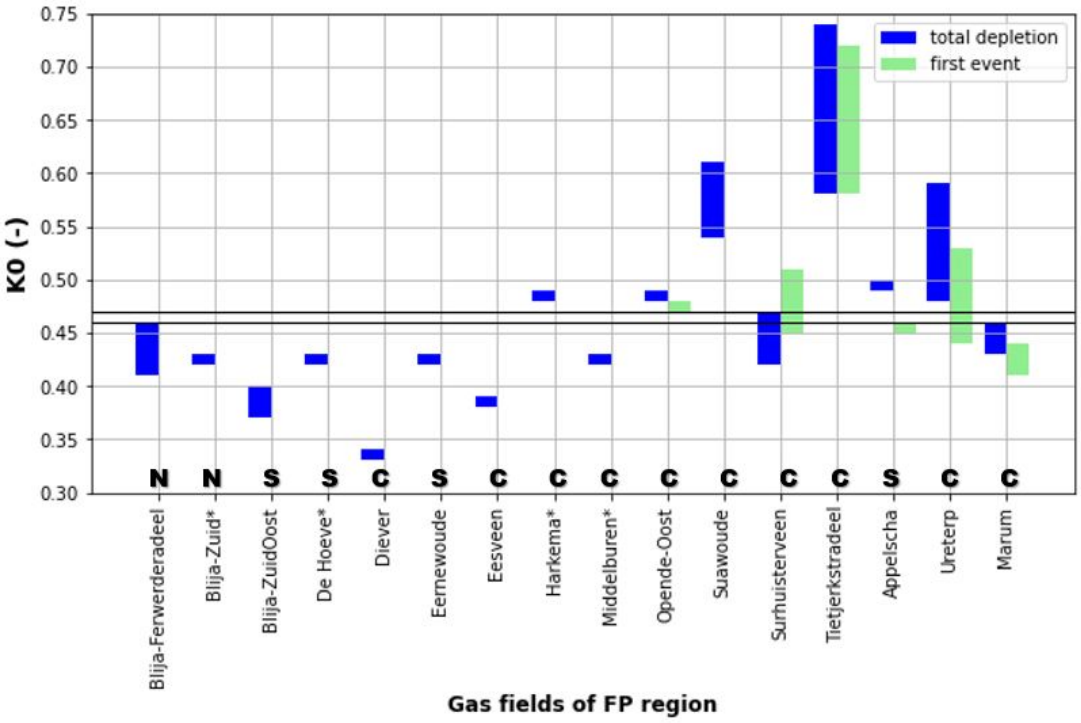

Figure 46: FP K0 bars (N = North, C = Central, S = South

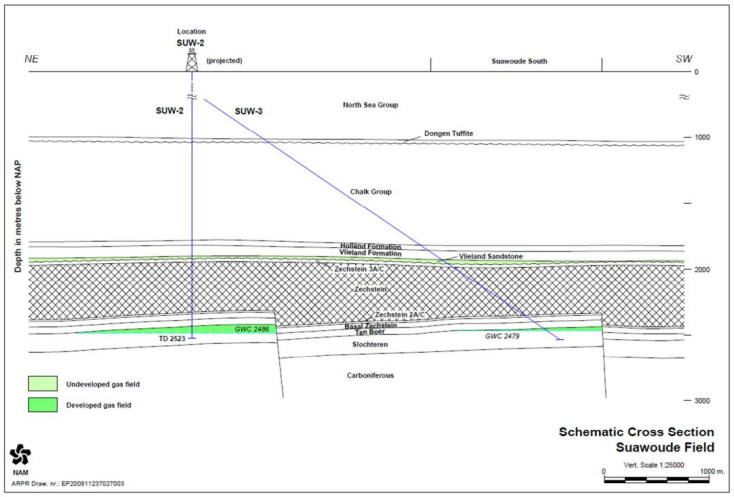

Figure 47: Cross section of Suawoude (NAM, 2012)

8.1.5 Lauwerszee Trough

The stress ratio ranges for each field in the LT region are shown in figure 48. The region is split into two regions, North and South, due to the wide variation in stress ratio's, which makes it difficult to identify a regional stress ratio. This strategy was adopted on the grounds that there would be more similar reservoir features in a smaller region.

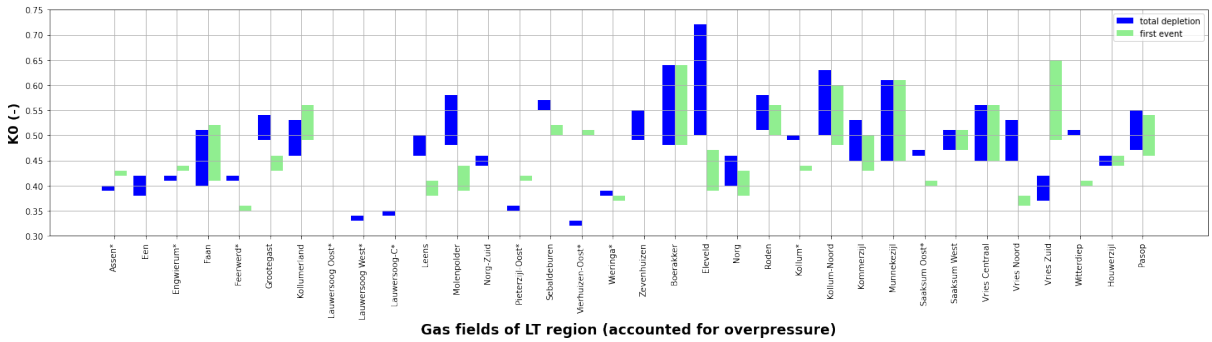

Figure 48: LT K0 range

There are 13 fields in the North and 10 fields in the South after the fields without internal faults are disregarded due to a lack of internal faults. Now the results in the North area will be discussed. Faan should definitely not become seismically active. Kollumerland is associated with events that are more likely caused by Grootegast and Kollum-Noord. The seismic event linked to Sebaldeburen is more likely associated with Boerakker. Pasop is linked to two seismic events, the first one is a better fit with Vries-Noord and the second one with Boerakker. For Grootegast it could also be that that event is wrongly associated with the gas field. The seismic event could be better matched with either Grijpskerk or Kommerzijl. The seismic event associated with Leens should most likely be linked to Houwerzijl or Saaksum-West. For Witterdiep, it is possible that the event is not the actual first event, but rather a second event. The first event could be related to another field, most likely to Eleveld due to its seismic activity and proximity. The stress ratio range for Houwerzijl is relatively low, which could be due to the complex geology. As the first event may be related to a boundary fault between Leens and Saaksum-Oost. Hence Faan, Grootgast, Houwerzijl, Kollumerland, Leens, Pasop, Sebaldeburen and Witterdiep are assumed to be without any seismicity and therefore below the regional stress ratio.

The geology of Molenpolder is complex, as illustrated in Appendix A8. Intersecting faults are partially located inside the field. These faults cross in the northwest and southeast directions. Kollum-Noord and Munnekezijl are seismically active fields and have relatively high stress ratio ranges. Saaksum-West has more complex geology possibly due to a boundary fault with Kommerzijl. It is assumed to be seismically active. Based on the findings in figure 49 of the North LT region, a regional stress ratio of 0.50 was chosen.

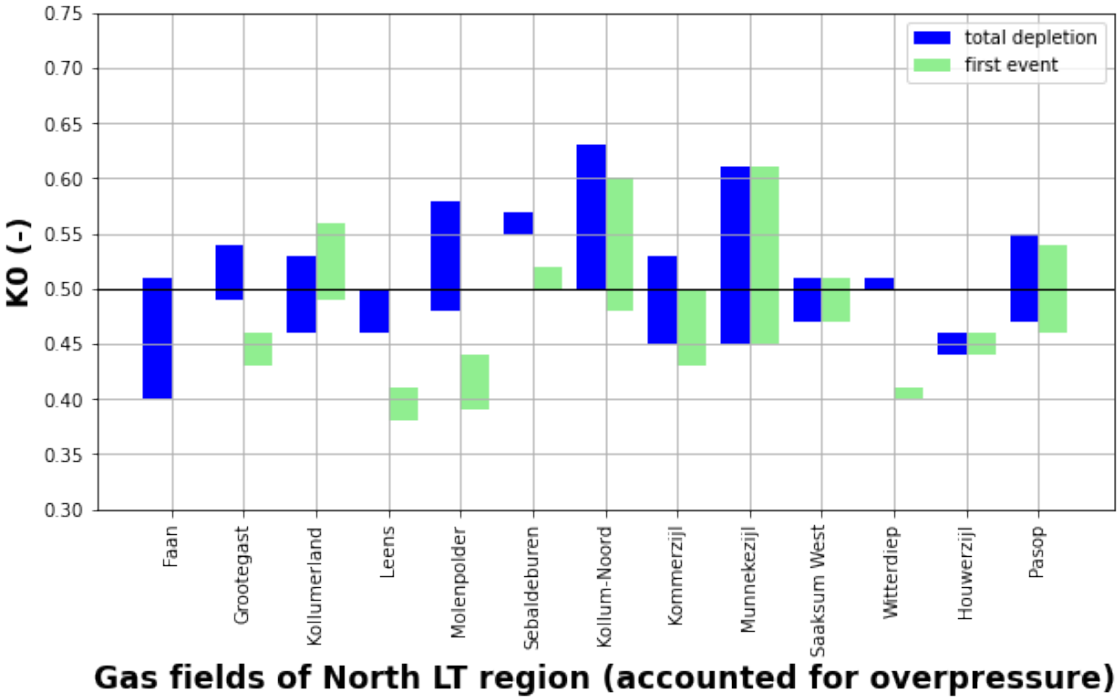

Figure 49: North LT K0 range with threshold

In total 10 fields are located in the South area, see figure 50. Een, Norg-Zuid and Zevenhuizen are not seismically active and have a relatively low stress ratio. For Vries Noord the stress ratio for the first event is quite low. It is possible that the event is not the actual first event, but rather related to another field, such as Roden. Hence, it is not responsible for seismicity. For Vries Zuid the stress ratio ranges are very low. The first event of Vries Zuid is also very close to Vries Centraal. Hence, the event may be related to Vries Centraal. One more event is also in close proximity to Vries Zuid, but it is also near Vries Centraal and Annerveen. So that event might be related to one of these two fields, implying that Vries Zuid lacks seismicity. The Norg gas field has complex structural geology with a large maximum offset of 100 meters. Currently, it is being used for gas storage, which could explain the low stress ratio. The first seismic event associated with Norg is better matched with Roden.

Boerakker, Eleveld, Roden and Vries Centraal are definitely seismically active with relatively high stress ratio's. Based on these results a regional stress ratio of 0.56 was chosen.

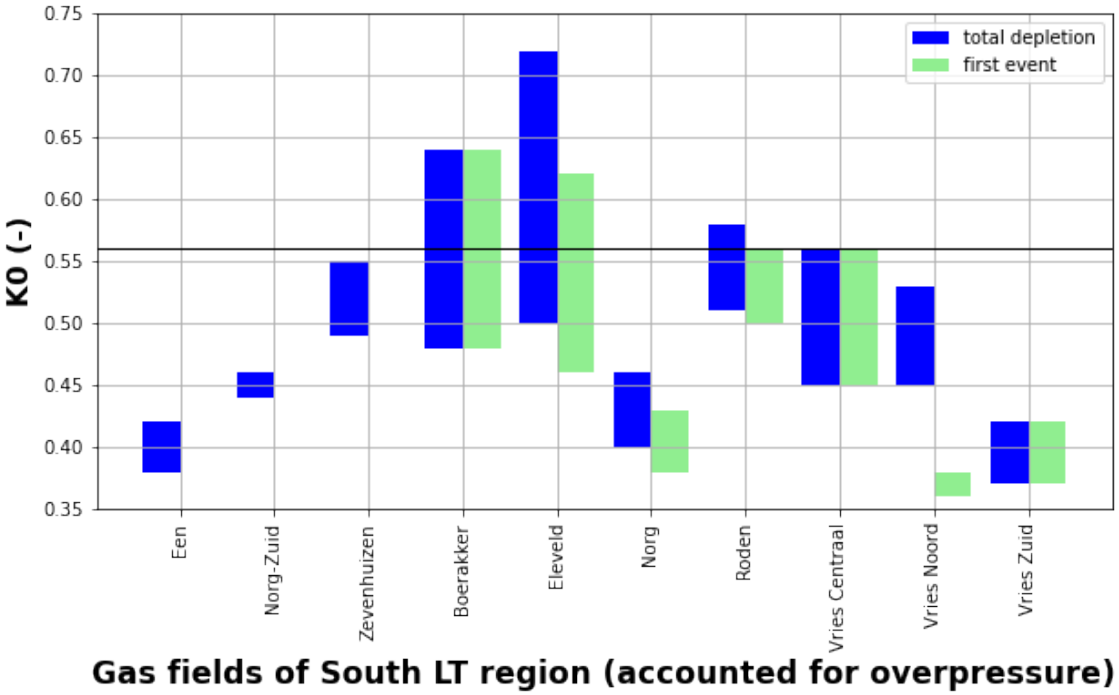

Figure 50: South LT K0 range

8.2 Uncertainties

The conclusions are based on several forms of data that contain various inaccuracies, the most significant of which will be highlighted in this section.

- Data inaccuracies and rounding errors might result in less reliable findings. Production plans from NLOG provide reservoir properties data such as the compaction coefficient. Some of this data predates 2014 and was collected using less precise methods. Furthermore, the geologic maps from NLOG were used to calculate absolute offsets based on contourlines.
- The K0 results are obtained with a Dc of 0.001. Due to instabilities in the model an intermediate value of 0.005 could not be used. So either 0.001 or 0.01 needed to be picked. In order to be conservative 0.001 was chosen, because this would overestimate the risk of seismicity.
- In the sensitivity analysis model instabilities made it difficult to properly understand the behaviour of several parameters.
- In 1986 seismic monitoring was initiated for events with magnitudes larger than 2.5. Hence, it leads to uncertainties in the field classification. Furthermore, the seismic monitoring did not cover the entire country of the Netherlands.

9 Conclusion

The research question was "Can the reservoir properties of small gas fields in the Netherlands predict the occurrence of seismicity?". The answer is yes, based on reservoir data and fault characteristics, it is possible to predict whether seismicity will occur in a small Dutch gas field located in the Rotliegend formation. This study showed that of the parameters influencing the onset of seismic slip on a reservoir fault the initial stress ratio and the Poisson's ratio are the most distinctive. The Poisson's ratio is not an appropriate parameter, because it is related to the compaction coefficient which is already predetermined for each gas field. For that reason, the stress ratio is the most sensitive parameter and has taken center stage. The regional stress ratio was determined for five structural regions with small gas fields that can define the (non-) occurrence of seismicity in a gas field. The regional stress ratio was 0.51 for NHP, 0.58 for Groningen, 0.69 for LTHP, 0.46 and 0.47 for FP and 0.50 and 0.55 for LT. Moreover, the

relatively thick salt deposits above Groningen and LTHP most probably contributed to the increase in the regional stress ratio, because salt increases the effective horizontal and vertical stresses. For further research I suggest to analyze other formations, such as Zechstein. The model instabilities limited the comprehension of the sensitivity analysis for the dynamic friction coefficient, fault dip angle and static friction coefficient. Improvements to the code will help to increase the validity.

10 References

Altmann, J. B. (2010). Poroelastic effects in reservoir modelling (Doctoral dissertation, Karlsruher Inst. für Technologie, Diss.

Arfai, J., Franke, D., Lutz, R., Reinhardt, L., Kley, J., & Gaedicke, C. (2018). Rapid Quaternary subsidence in the northwestern German North Sea. Scientific Reports, 8(1). doi: 10.1038/s41598-018-29638-6

Beaumont, E., & Foster, N. (1999). Exploring for Oil and Gas Traps. doi: 10.1306/trhbk624

Buijze, L., van den Bogert, P., Wassing, B., Orlic, B.,& ten Veen, J. (2017). Fault reactivation mechanisms and dynamic rupture modelling of depletion-induced seismic events in a Rotliegend gas reservoir. Netherlands Journal Of Geosciences, 96(5), s131-s148. doi: 10.1017/njg.2017.27

De Waal, Hans & Roest, J.P.A. & Fokker, Peter & Kroon, I. & Breunese, J.N. & Muntendam-Bos, Annemarie G. & Oost, Albert & van Wirdum, Geert. (2012). The effective subsidence capacity concept: How to assure that subsidence in the Wadden Sea remains within defined limits?. Geologie en Mijnbouw. Neth. Journ. Of Geosc.,. 385-399. 10.1017/S0016774600000512.

Dost, B., & Kraaijpoel, D. (2013). The August 16, 2012 earthquake near Huizinge (Groningen). KNMI Scientific Report. Royal Netherlands Meteorological Institute (KNMI), Utrecht, The Netherlands.

Doyle, P. (2008). England's Heritage in Stone.

Duin, E. J. T., et al. Subsurface structure of the Netherlands-results of recent onshore and offshore mapping. Netherlands Journal of Geosciences, 2006, 85.4: 245.

Gambolati, G. & Ferronato, M. & Teatini, P. (2006). Reservoir compaction and land subsidence. Revue européenne de génie civil. 10. 731-762. 10.1080/17747120.2006.9692854.

Geluk, M.C., 2005. Stratigraphy and tectonics of Permo-Triassic basins in the Netherlands and surrounding areas. PhD thesis, University of Utrecht: 171 pp.

Groningen gasveld | NLOG. (n.d.). https://www.nlog.nl/groningen-gasveld

Herber, R., De Jager, J. (2010). Geoperspective Oil and Gas in the Netherlands–Is there a future?. Netherlands Journal of Geosciences, 89(2), 91-107. https://www.knmi.nl/over-het-knmi/about

Jansen, J. D., Singhal, P., Vossepoel, F. C. (2019). Insights from closed-form expressions for injection-and production-induced stresses in displaced faults. Journal of Geophysical Research: Solid Earth, 124(7), 7193-7212. Jansen, J., Meulenbroek, B. (2022). Induced aseismic slip and the onset of seismicity in displaced faults. Netherlands Journal of Geosciences, 101, E13. doi:10.1017/njg.2022.9

Kortyna, C., DeCelles, P. G., Carrapa, B. (2019). Structural and thermochronologic constraints on kinematics and timing of inversion of the Salta rift in the Tonco-Amblayo sector of the Andean retroarc fold-thrust belt, northwestern Argentina. In Andean tectonics (pp. 429-464). Elsevier.

KNMI - Aardbevingen door gaswinning. (2022). Retrieved July 2022, from https://www.knmi.nl/kennis-en-datacentrum/uitleg/aardbevingen-door-gaswinning

KNMI - Aardbevingen door gaswinning. (n.d.). https://www.knmi.nl/kennis-en-datacentrum/uitleg/aardbevingen-door-gaswinning

KNMI - About KNMI. (n.d.).

KNMI - Eerste seismische registratie De Bilt. (n.d.). https://www.knmi.nl/kennis-en-datacentrum/uitleg/eerste-seismische-registratie-de-bilt

KNMI - Jaaroverzicht aardbevingen 2021. (2022). Retrieved July 2022, from https://www.knmi.nl/over-het-knmi/nieuws/jaaroverzicht-aardbevingen-2021: :text=In%20Nederland%20waren%

Kombrink, H. (2008). The Carboniferous of the Netherlands and surrounding areas; a basin analysis. Geologica Ultraiectina (294). Departement Aardwetenschappen

Matrullo, E. (2012). Fault delineation and stress orientations from the analysis of background, low magnitude seismicity in Southern Apennines (Italy).

McBeck, J., Mair, K., & Renard, F. (2019). How porosity controls macroscopic failure via propagating fractures and percolating force chains in porous granular rocks. Journal of Geophysical Research: Solid Earth, 124(9), 9920-9939.

Mckie, T. (2011). A comparison of modern Dryland depositional systems with the Rotliegend group in the Netherlands. SEPM Special Publications. 98. 89-103. 10.2110/pec.11.98.0089.

Ministerie van Economische Zaken en Klimaat. (2021). Olie- en gaswinning. Sectoren | Staatstoezicht Op De Mijnen. https://www.sodm.nl/sectoren/olie–en-gaswinning

Muntendam-Bos, A. (2021). Geomechanical characteristics of gas depletion induced seismicity in the Netherlands. American Rock Mechanics Association.

Muntendam-Bos, A. G. (2021, June). Geomechanical characteristics of gas depletion induced seismicity in The Netherlands. In 55th US Rock Mechanics/Geomechanics Symposium. OnePetro.

Muntendam-Bos, A. G. (2021, June). Geomechanical characteristics of gas depletion induced seismicity in The Netherlands. In 55th US Rock Mechanics/Geomechanics Symposium. OnePetro.

Muntendam-Bos, A., Hoedeman, G., Polychronopoulou, K., Draganov, D., Weemstra, C., & van der Zee, W. et al. (2022). An overview of induced seismicity in the Netherlands. Netherlands Journal Of Geosciences, 101. doi: 10.1017/njg.2021.14

Nelskamp, S., Verweij, J., & Witmans, N. (2012). The role of salt tectonics and overburden in the generation of overpressure in the Dutch North Sea area. Netherlands Journal of Geosciences - Geologie En Mijnbouw, 91(4), 517-534. doi:10.1017/S0016774600000366

Oil and gas | NLOG. (n.d.). https://www.nlog.nl/en/oil-and-gas

Raziperchikolaee, S., Singh, V., Kelley, M. (2020). The effect of Biot coefficient and elastic moduli stress–pore pressure dependency on poroelastic response to fluid injection: laboratory experiments and geomechanical modeling. Greenhouse Gases: Science and Technology, 10(5), 980-998. Retrieved September 2019, from https://www.geoexpro.com/articles/2009/04/the-groningen-gas-field

Sainoki, A., & Mitri, H. (2015). Effect of slip-weakening distance on selected seismic source parameters of mining-induced fault-slip. International Journal Of Rock Mechanics And Mining Sciences, 73, 115-122. doi: 10.1016/j.ijrmms.2014.09.019

Slowakiewicz, M, Blumenberg, M.,Więcław, D., Hindenberg, K. & Röhling, H., Scheeder, G.. Idiz, E., Tucker, M., Pancost, R., Kotarba, M. & Gerling, J.. (2017). Zechstein 2 oil characteristics in the Southern Permian Basin of Europe: The role of C40 carotenoids.

Słowakiewicz, M., Tucker, M. E., Perri, E., & Pancost, R. D. (2015). Nearshore euxinia in the photic zone of an ancient sea. Palaeogeography, Palaeoclimatology, Palaeoecology, 426, 242-259.

Strozyk, F., Reuning, L., Scheck-Wenderoth, M., & Tanner, D. (2017). The Tectonic History of the Zechstein Basin in the Netherlands and Germany. Permo-Triassic Salt Provinces Of Europe, North Africa And The Atlantic Margins, 221-241. doi: 10.1016/b978-0-12-809417-4.00011-2

TNO-NITG, 2004. Geological Atlas of the Subsurface of the Netherlands – onshore: 103 pp.

Van den Bogert, P. A. J. (2018) Depletion-induced fault slip and seismic rupture. NAM

Van den Bogert, P. A. J., & van Eijs, R. M. H. E. (2020). Why Mohr-circle analyses may underestimate the risk of fault reactivation in depleting reservoirs. International Journal of Rock Mechanics and Mining Sciences, 136, 104502.

van Thienen-Visser, K., & Breunese, J. N. (2015). Induced seismicity of the Groningen gas field: History and recent developments. The Leading Edge, 34(6), 664-671.

van Thienen-Visser, K., Roholl, J. A., van Kempen, B. M. M., Muntendam-Bos, A. G. (2018). Categorizing seismic risk for the onshore gas fields in the Netherlands. Engineering Geology, 237, 198-207.

Verdoes, A., & Boin, A. (2021). Earthquakes in Groningen: Organized Suppression of a Creeping Crisis. Understanding The Creeping Crisis, 149-164. doi: 10.1007/978-3-030-70692-0-9

Verweij, J.M., T.A. Boxem, and S. Nelskamp. 2016. 3D spatial variation in vertical stress in on- and offshore Netherlands; integration of density log measurements and basin modelling results. Mar. Pet. Geol. 78, 870-882.

Verweij, J.M. & Simmelink, HJ & Underschultz, Jim. (2011). Pressure and fluid flow systems in the Permian Rotliegend in the Netherlands onshore and offshore. Society for Sedimentary Geology Special Publication. 98. 247-263. 10.2110/pec.11.98.0247.

Voigt, T., Kley, J., and Voigt, S.: Dawn and dusk of Late Cretaceous basin inversion in central Europe, Solid Earth, 12, 1443–1471, https://doi.org/10.5194/se-12-1443-2021, 2021.

Whaley, J. (2009). The Groningen Gas Field. GEO ExPro.

Appendices

The appendix contains input and output data, code for 3D representation with two parameters, cross sections, structural maps and J ratio histograms.

A 3D representation Jupyter Notebook trade-off between two parameters

```
#Code for 3D representation of two parameters versus pressure change
#Author Salima Oumejjoud
#Libraries
import numpy as np
import matplotlib.pyplot as plt
from mpl_toolkits.mplot3d import Axes3D
import pandas as pd
from matplotlib import cm
import plotly
import plotly.graph_objs as go
import plotly.graph_objects as go
#import data
dgro = pd.read_excel(r'C:\Users\salim\Desktop\thesis\K Dc data py.xlsx',sheet_name='Gro2')
Gro = dgro.to_numpy()
# Arrays x, y and z for data plot visualization
x = ([.3, .3667, .4333,.5,.5667,.6333,.7,.7667,.8333,.9])
y = np.linspace(0.001,0.01,10)
G1 = Gro[1:11,1:]
G2 = Gro[13:23,1:]
# meshgrid makes a rectangular grid out of two 1-D arrays.
x, y = np.meshgrid(x, y)
z1 = G1.astype(np.float)
z2 = G2.astype(np.float)
xw = x.flatten()
yw = y.flatten()
z1w = z1.flatten()
z2w = z2.flatten()
h1 = 36.3
h2 = 36.3
#1 Blijham with relative offset=0.05
#2 Blijham K & Dc analysis with max relative offset
#plot plane
z= h10*np.ones((100,75)) # <-- Put your data
x = ([.3, .3667, .4333,.5,.5667,.6333,.7,.7667,.8333,.9])
y = np.linspace(0.001,0.01,10)
mycolorscale = [[0, '#aa9ce2'],[1, '#aa9ce2']]
surf = go.Surface(x=x, y=y, z=z, colorscale=mycolorscale, showscale=False)
layout = go.Layout(width=600,scene_camera_eye_z=0.75)
fig = go.Figure(data=[surf], layout=layout)
# meshgrid makes a rectangular grid out of two 1-D arrays.
x1, y1 = np.meshgrid(x, y)
# Configure Plotly to be rendered inline in the notebook.
plotly.offline.init_notebook_mode()
# Configure the trace.
trace = go.Scatter3d(x =xw,y =yw,z=z10w, # <-- Put your data
mode='markers',marker={'size': 10,'opacity': 0.8,})
# Configure the layout.
layout = go.Layout( margin={'l': 0, 'r': 0, 'b': 0, 't': 0})
data = [trace]
surf = go.Surface(x=x, y=y, z=z, colorscale=mycolorscale, showscale=False)
data1 = [trace,surf]
plot_figure = go.Figure(data1, layout=layout)
# Render the plot.
plotly.offline.iplot(plot_figure)
```

B Input and output data examples of porosity and gas field Groet

porosity																			
	0.05		0.0833		0.1167		0.15		0.1833		0.2167		0.25		0.2833		0.3167		0.35
0.05	-30	0.05	-30	0.05	-30	0.05	-30	0.05	-30	0.05	-30	0.05	-30	0.05	-30	0.05	-30	0.05	-30
0.15	-30	0.15	-30	0.15	-30	0.15	-30	0.15	-30	0.15	-30	0.15	-30	0.15	-30	0.15	-30	0.15	-30
0.25	-30	0.25	-30	0.25	-30	0.25	-30	0.25	-30	0.25	-30	0.25	-30	0.25	-30	0.25	-30	0.25	-30
0.35	-30	0.35	-30	0.35	-30	0.35	-30	0.35	-30	0.35	-30	0.35	-30	0.35	-30	0.35	-30	0.35	-30
0.45	-30	0.45	-30	0.45	-30	0.45	-30	0.45	-30	0.45	-30	0.45	-30	0.45	-30	0.45	-30	0.45	-30
0.55	-30	0.55	-30	0.55	-30	0.55	-30	0.55	-30	0.55	-30	0.55	-30	0.55	-30	0.55	-30	0.55	-30
0.65	-30	0.65	-30	0.65	-30	0.65	-30	0.65	-30	0.65	-30	0.65	-30	0.65	-30	0.65	-30	0.65	-30
0.75	-30	0.75	-30	0.75	-30	0.75	-30	0.75	-30	0.75	-30	0.75	-30	0.75	-30	0.75	-29.299	0.75	-28.163
0.85	-30	0.85	-30	0.85	-30	0.85	-30	0.85	-30	0.85	-29.145	0.85	-28.107	0.85	-27.063	0.85	-26.014	0.85	-24.957
0.95	-27.119	0.95	-26.2	0.95	-25.131	0.95	-24.505	0.95	-23.577	0.95	-22.687	0.95	-21.699	0.94	-21.789	0.95	-20.016	0.95	-19.13

Table 5: Porosity vs normalised offset with pressure results in MPa (marked in orange means error included)

Groet th = 0.05																				
	K & Dc																			
Dc , K -->	0.3		0.3667		0.4333		0.5		0.5667		0.6333		0.7		0.7667		0.8333		0.9	
0.001		0.001	7.0069	0.001	15.5085	0.001	24.0091	0.001	32.5094	0.001	41.0095	0.001	49.5097	0.001	50	0.001	50	0.001	50	
0.002		0.002	7.0069	0.002	15.5085	0.002	24.0091	0.002	32.5094	0.002	41.0095	0.002	49.5097	0.002	50	0.002	50	0.002	50	
0.003		0.003	7.3735	0.003	15.6792	0.003	24.0093	0.003	32.5094	0.003	41.0095	0.003	49.5097	0.003	50	0.003	50	0.003	50	
0.004		0.004	7.9566	0.004	16.808	0.004	24.8978	0.004	32.5345	0.004	41.0097	0.004	49.5097	0.004	50	0.004	50	0.004	50	
0.005		0.005	8.465	0.005	17.7959	0.005	26.2301	0.005	34.1498	0.005	41.6001	0.005	49.52	0.005	50	0.005	50	0.005	50	
0.006		0.006	8.9167	0.006	18.9716	0.006	27.4509	0.006	35.6600	0.006	43.4149	0.006	50	0.006	50	0.006	50	0.006	50	
0.007		0.007	9.3271	0.007	19.4705	0.007	28.5646	0.007	37.0247	0.007	45.0464	0.007	50	0.007	50	0.007	50	0.007	50	
0.008		0.008	9.7037	0.008	20.2049	0.008	29.5938	0.008	38.2863	0.008	46.5256	0.008	50	0.008	50	0.008	50	0.008	50	
0.009		0.009	10.0529	0.009	20.8847	0.009	30.5388	0.009	39.4681	0.009	47.9054	0.009	50	0.009	50	0.009	50	0.009	50	
0.01		0.01	10.3736	0.01	21.5173	0.01	31.4241	0.01	40.5787	0.01	49.2054	0.01	50	0.01	50	0.01	50	0.01	50	

Table 6: Stress ratio vs critical slip distance with relative offset of 0.05 with pressure results in MPa (marked in orange means error included)

Input field parameters (bold red = min&max artificial data; bold blue = min artificial data)													
reservoir name	P_ini (Mpa)	over-pressure [MPa]	Depletion 1st event (Mpa)	total depletion [MPa]	faults min	faults max	reservoir depth (m)	relative offset min	relative offset max	reservoir dikte (m)	cm (10-5/bar)	onset of production	date 1st event	class
Groet	23	1.44	18.8	21	0	10	2156	0	0.046296	216	0.63	1/1/1974	10/10/2001	C3
Groet-Oost	23.5	1.08		15	0	10	2242	0	0.046296	216	0.65	2/1/2006		C3
Middenmeer	21.8	2.8		1.8	0	10	1900	0.05	0.238095	42	0.3	7/1/1977		D
Rustenburg	25	3.5		14.5	10	50	2150	0.05	0.263158	190	0.51	9/1/2009		D
schermer (rot)	25.3	1.55		19.8	0	10	2375	0	0.046296	216	0.65	9/1/1979		D
Westbeemster	29	4		13.2	0	10	2500	0	0.067114	149	0.65	11/1/2007		D
Bergen ROSL	21.8	1.05	18.9	20.7	30	55	2075	0.15	0.275	200	0.57	10/13/1978	10/10/2001	C3
Bergermeer	22.8	1.08	16.4	20.8	10	100	2172	0.05	0.454545	220	0.53	9/1/1972	8/6/1994	B3
Middelie ROSL	27	2.5	11.5	11.5	25	125	2450	0.138889	0.694444	180	0.68	8/1/1975	12/1/1989	C3

exact								
	input					output		
						Pdep	P1st	dep	1st
	th min	th max	Pdep	P1st ev.		K0 min	K0 min	K0max	K0 max
Groet	0	0.046296296	21	18.8		-	-	0.47	0.46
Groet-Oost	0	0.0462963	15			-	-	0.42	-
Middenmeer	0.05	0.23809524	1.8			0.323	-	0.33	-
Rustenburg	0.05	0.26315789	14.5			0.43	-	0.5	-
schermer (rot)	0	0.0462963	19.8			-	-	0.45	-
Westbeemster	0	0.06711409	13.2			-	-	0.41	-
Bergen ROSL	0.15	0.275	20.7	18.9		**0.54**	0.51	0.58	0.55
Bergermeer	0.05	0.45454545	20.8	16.4		0.47	0.44	0.61	0.55
Middelie ROSL	0.13888889	0.69444444	11.5	11.5		0.42	0.42	0.49	0.49

Table 7: Input and exact output for NHP gas fields

C Geological maps: Cross sections

C.1 Vries Zuid

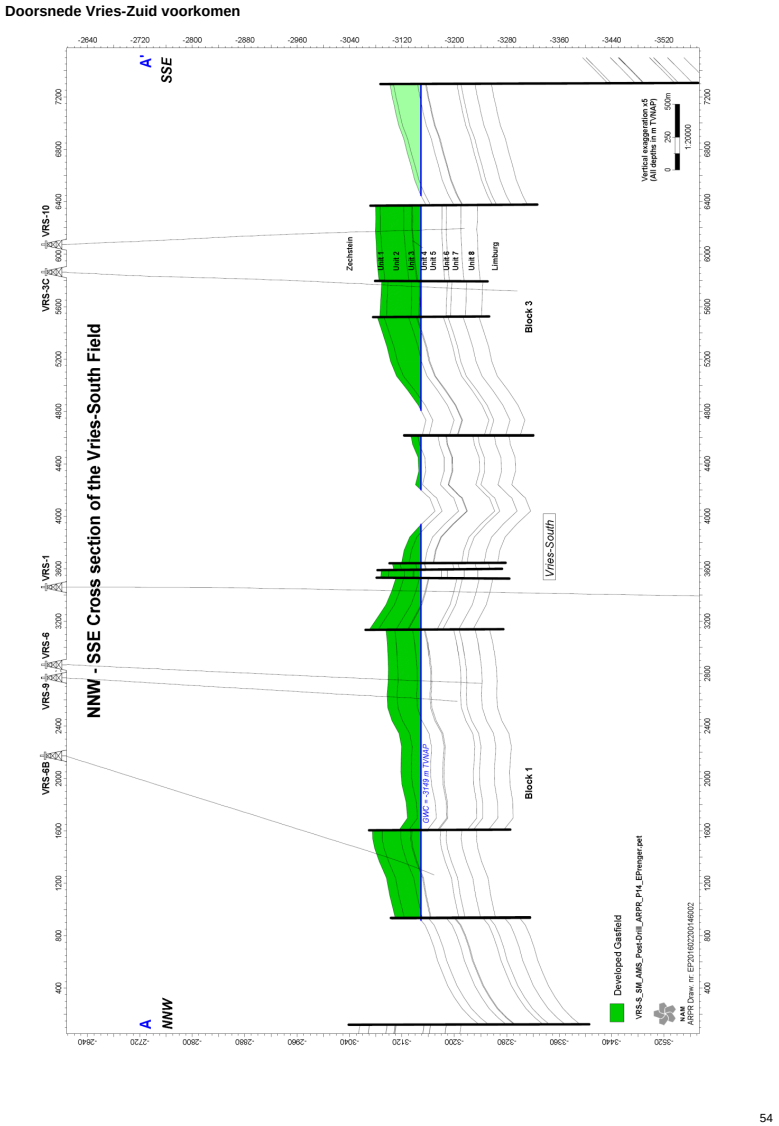

54

Figure A1: Cross section of Vries Zuid (NAM, 2016)

C.2 Vries Centraal & Noord

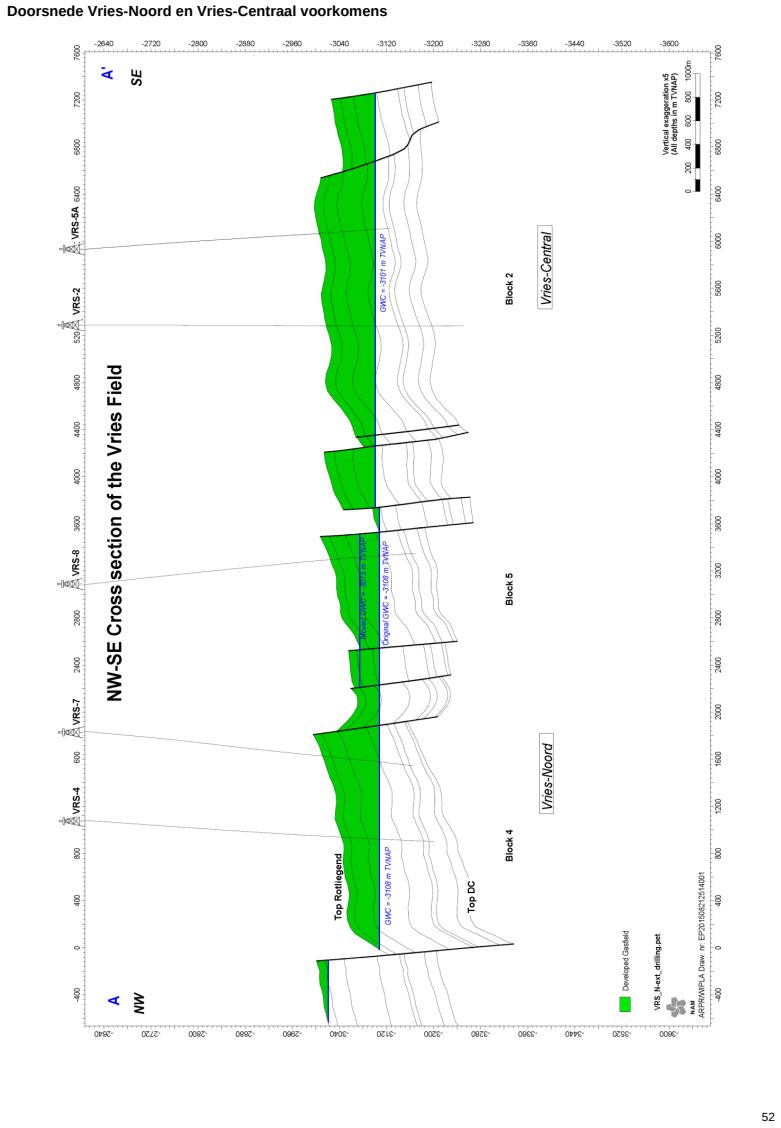

Figure A2: Cross section of Vries Centraal & Noord (NAM, 2016)

C.3 Witterdiep

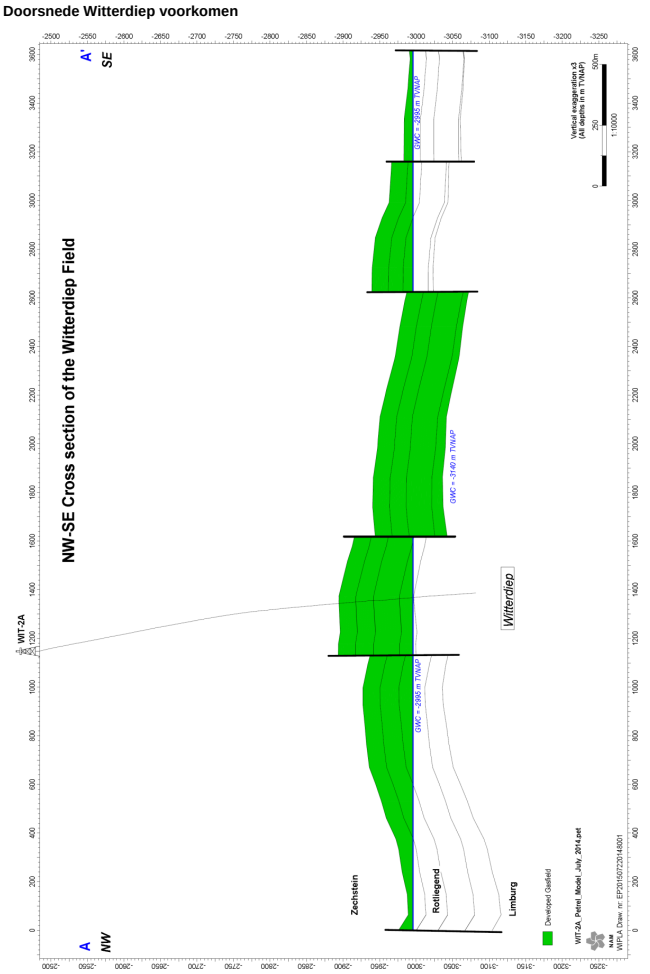

58

Figure A3: Cross section of Witterdiep (NAM, 2016)

D Geological maps: Structural maps

D.1 Ameland-Westgat

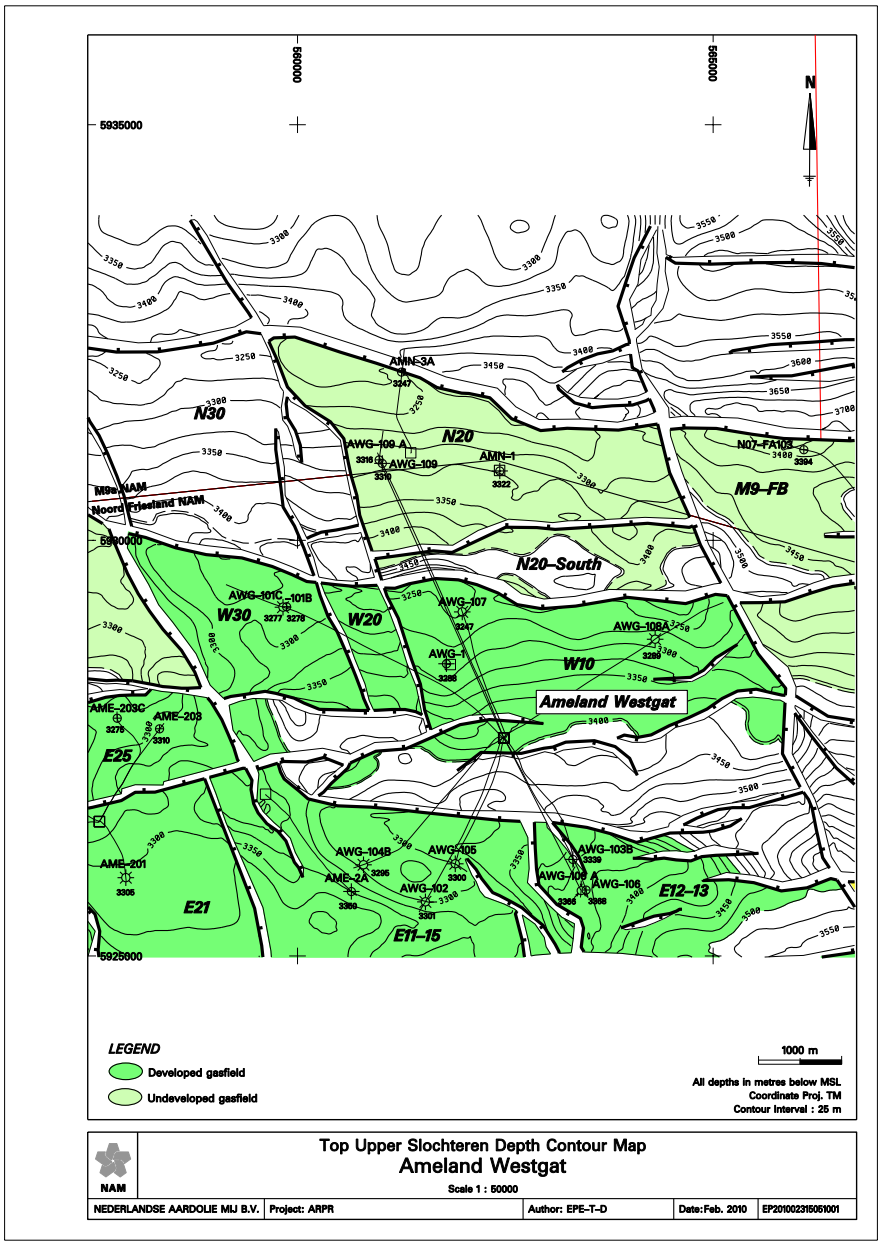

Figure A4: Structural map of Ameland-Westgat (NAM, 2010)

D.2 Rustenburg

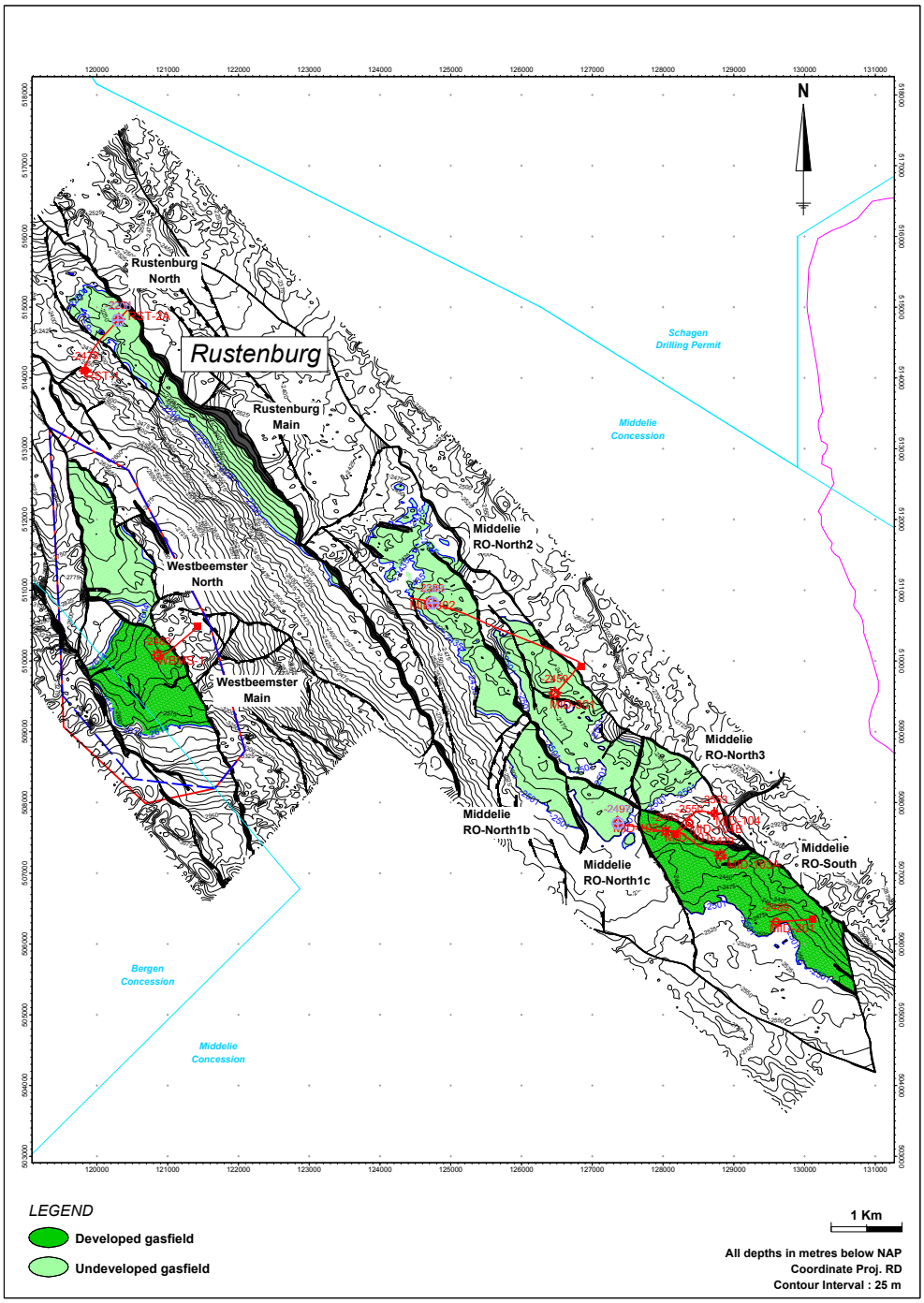

Figure A5: Structural map of Rustenburg (NAM, 2000)

D.3 Faan

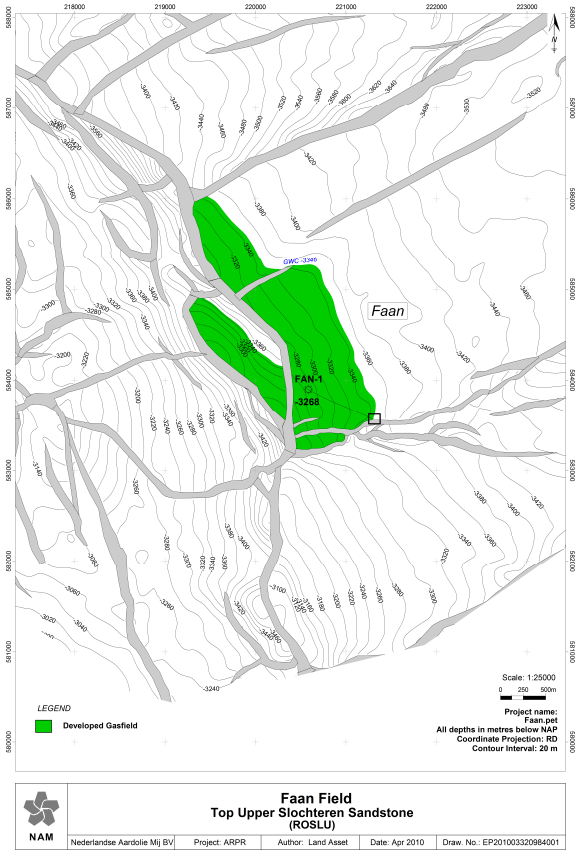

Figure A6: Structural map of Faan (NLOG, 2010)

D.4 Leens

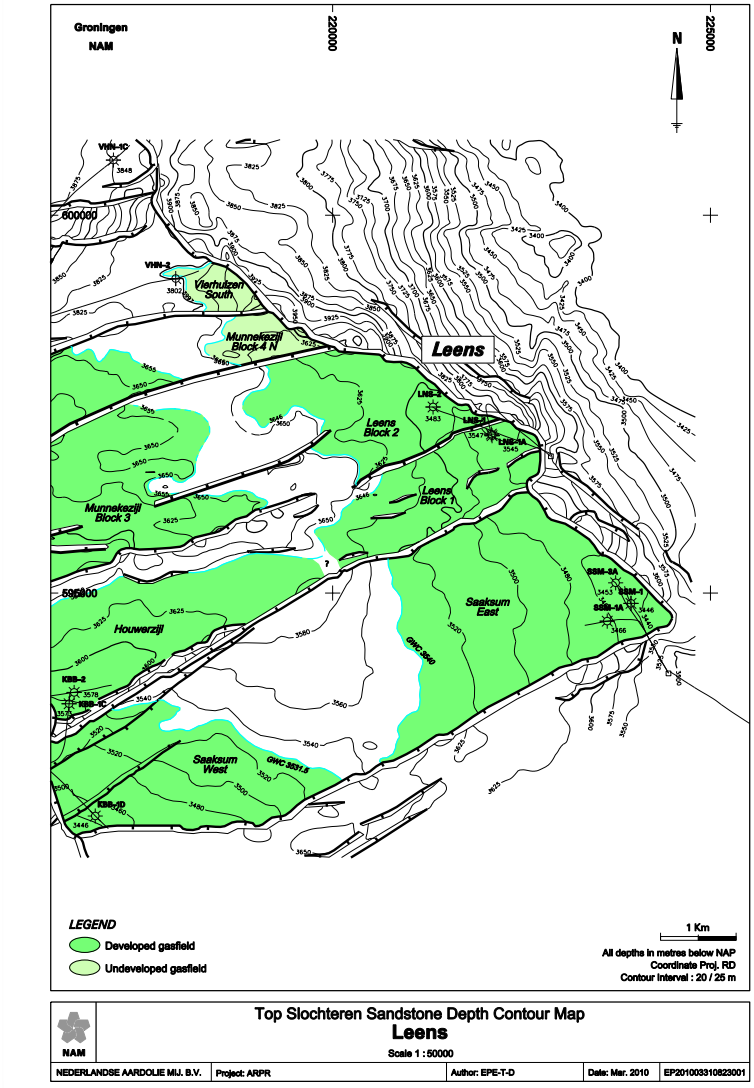

Figure A7: Structural map of Leens (NLOG, 2010)

D.5 Molenpolder

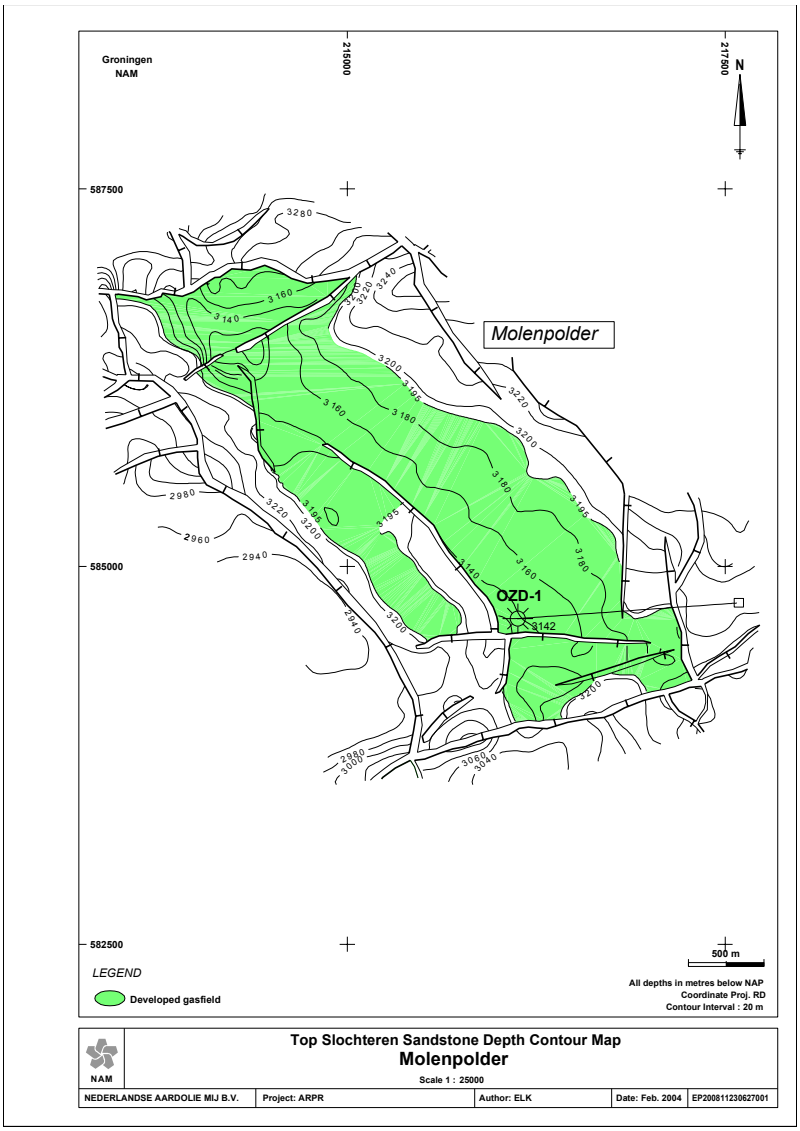

Figure A8: Structural map of Molenpolder (NLOG, 2004)

D.6 Norg-Zuid

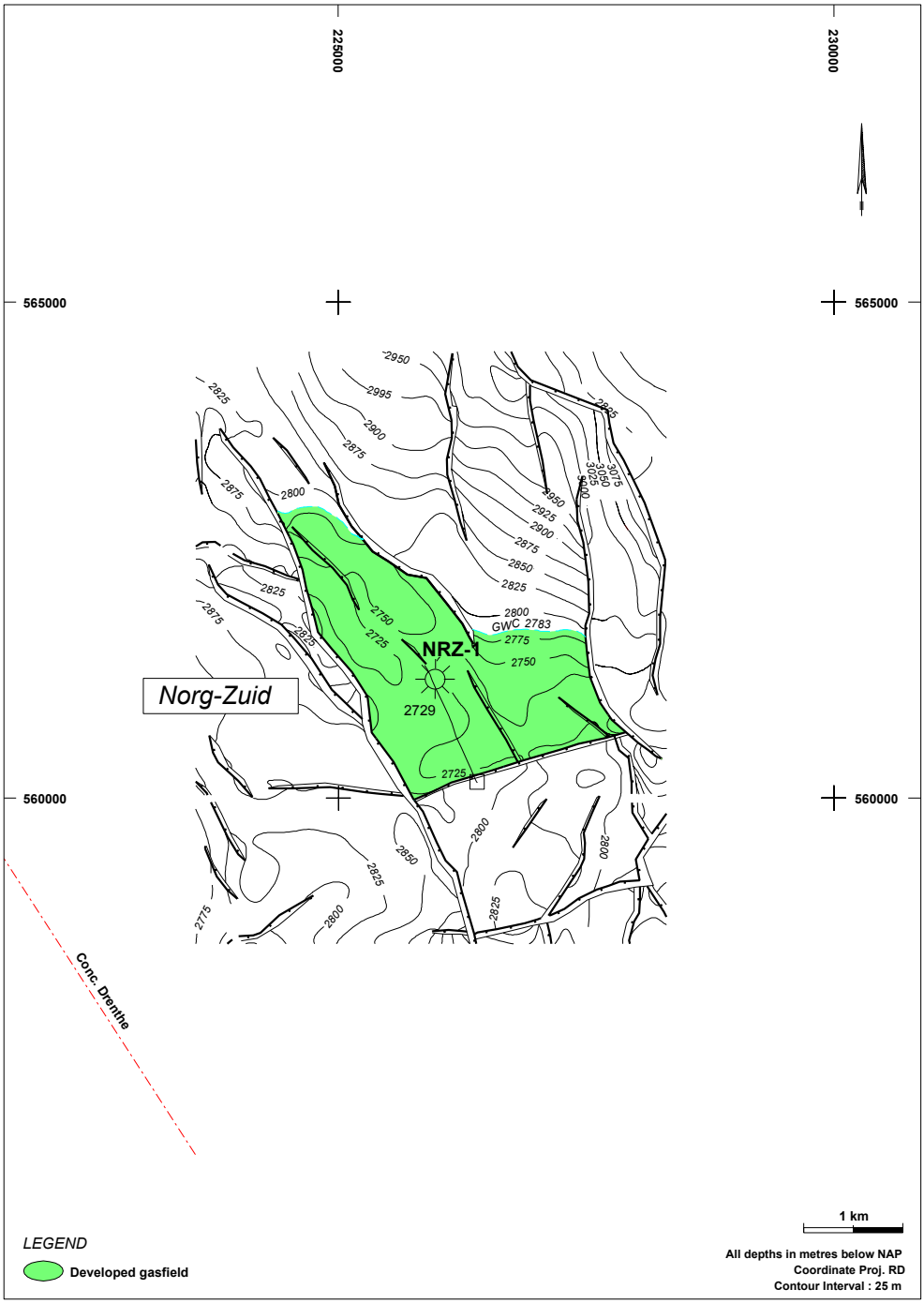

Figure A9: Structural map of Norg-Zuid (NLOG, 2005)

D.7 Zevenhuizen

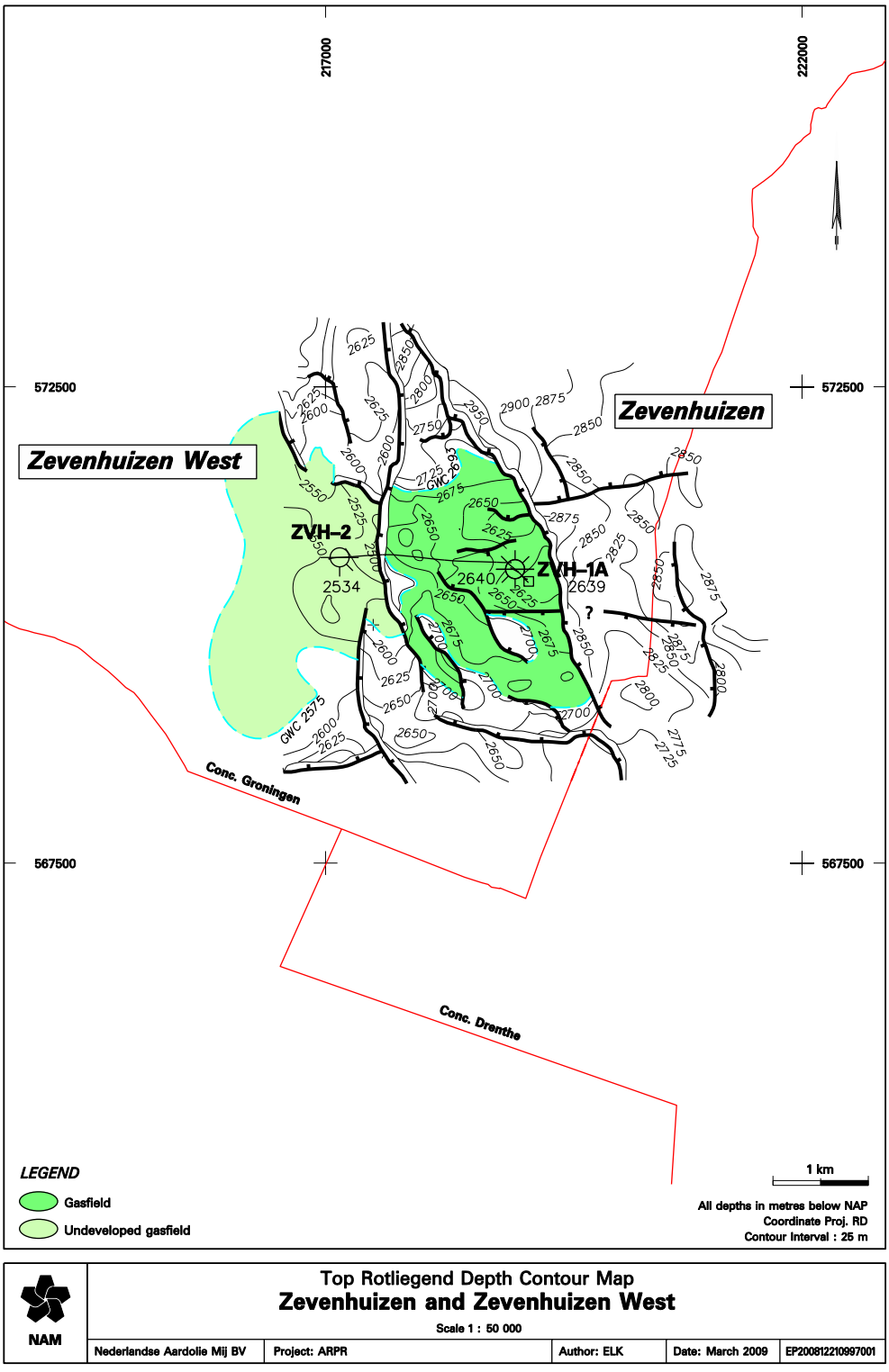

Figure A10: Structural map of Zevenhuizen (NLOG, 2009)

D.8 Norg

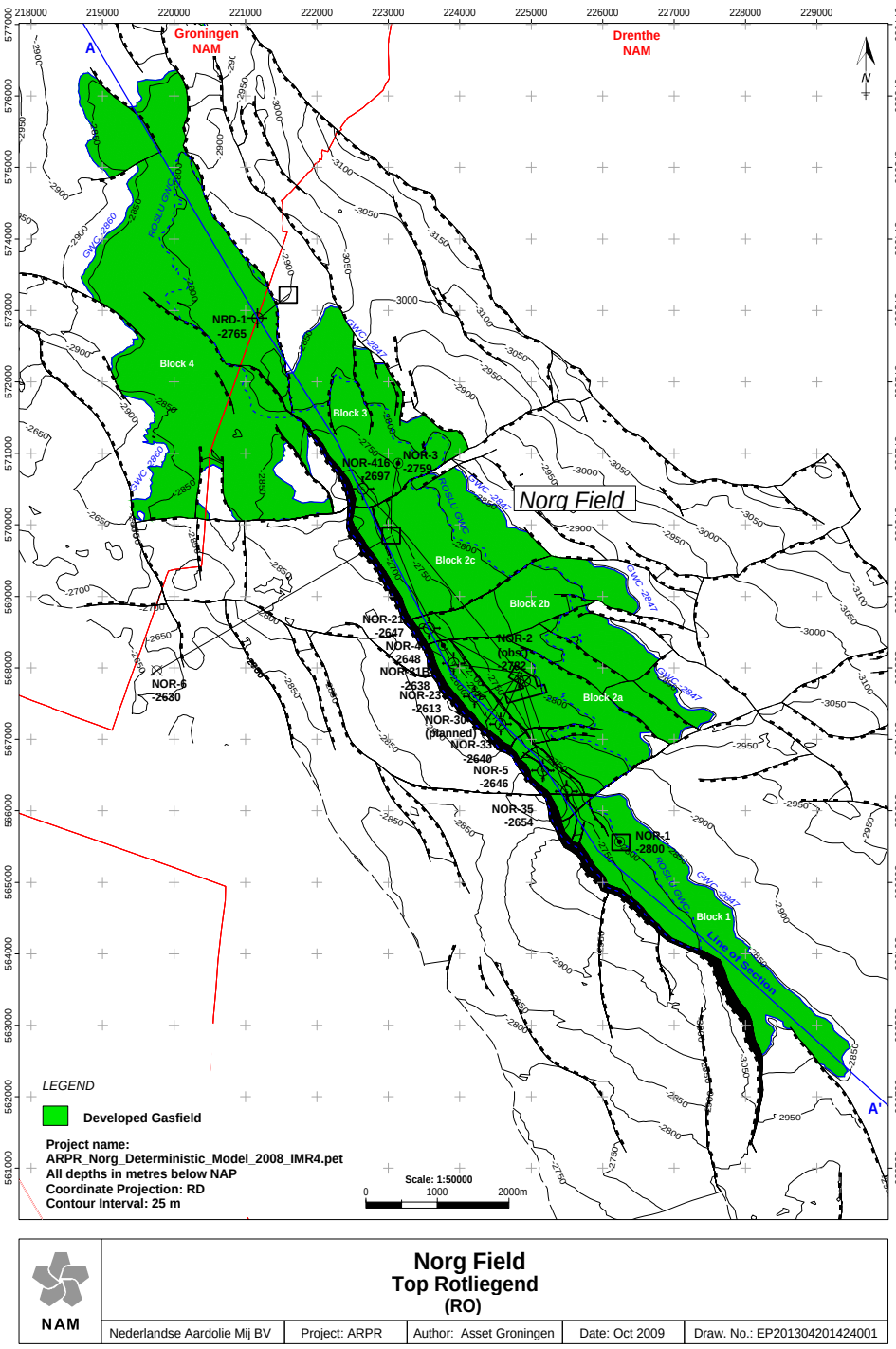

Figure A11: Structural map of Norg (NLOG, 2009)

D.9 Vries Centraal & Vries Noord

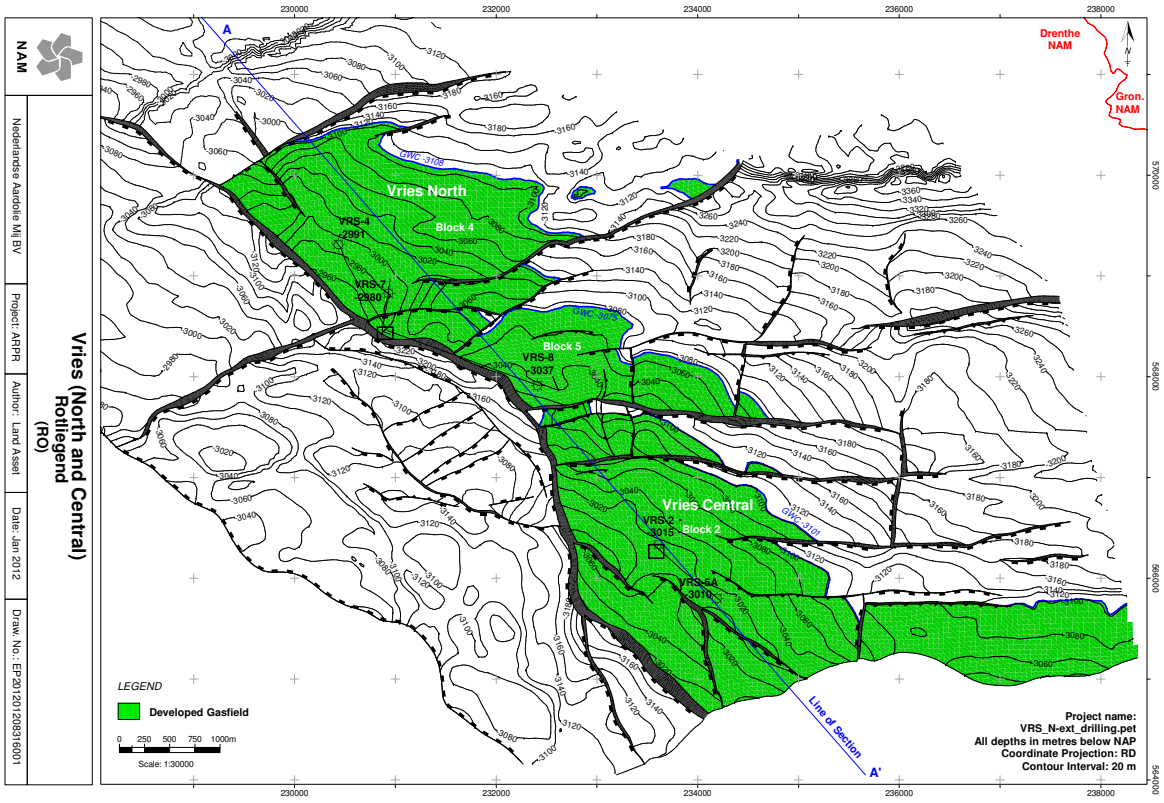

Figure A12: Structural map of Vries Centraal and Vries Noord (NLOG, 2012)

D.10 Vries Zuid

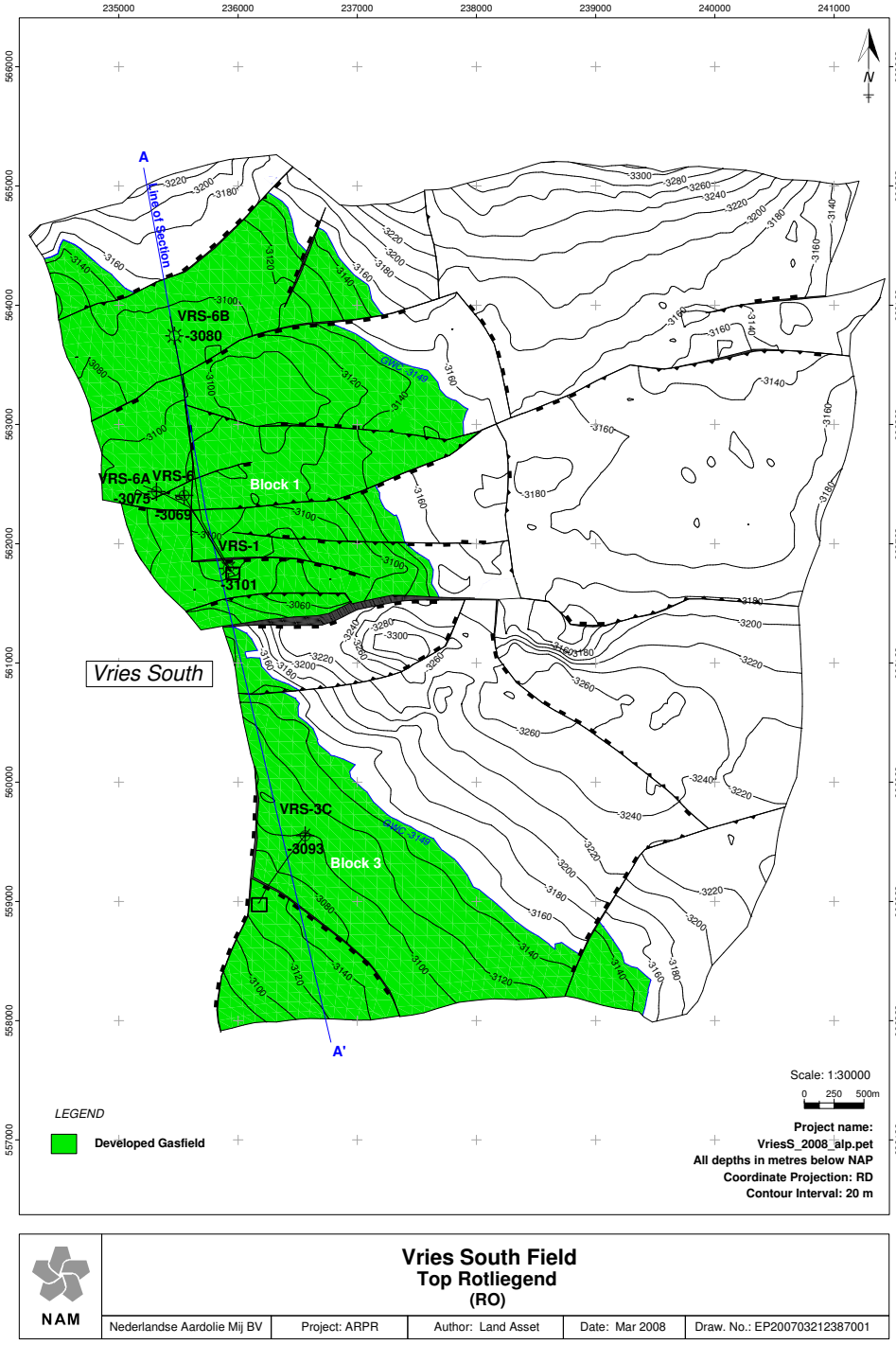

Figure A13: Structural map of Vries South (NLOG, 2008)

D.11 Witterdiep

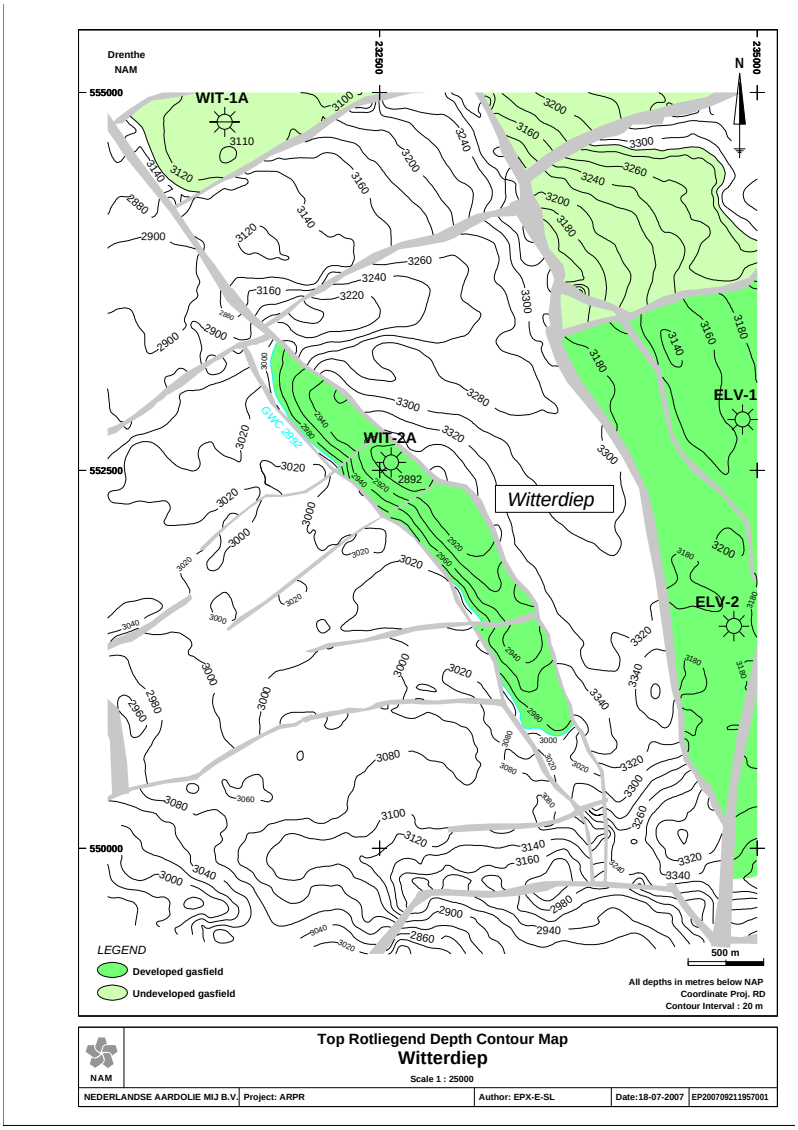

Figure A14: Structural map of Witterdiep (NLOG, 2007)

E J ratio

E.1 NHP

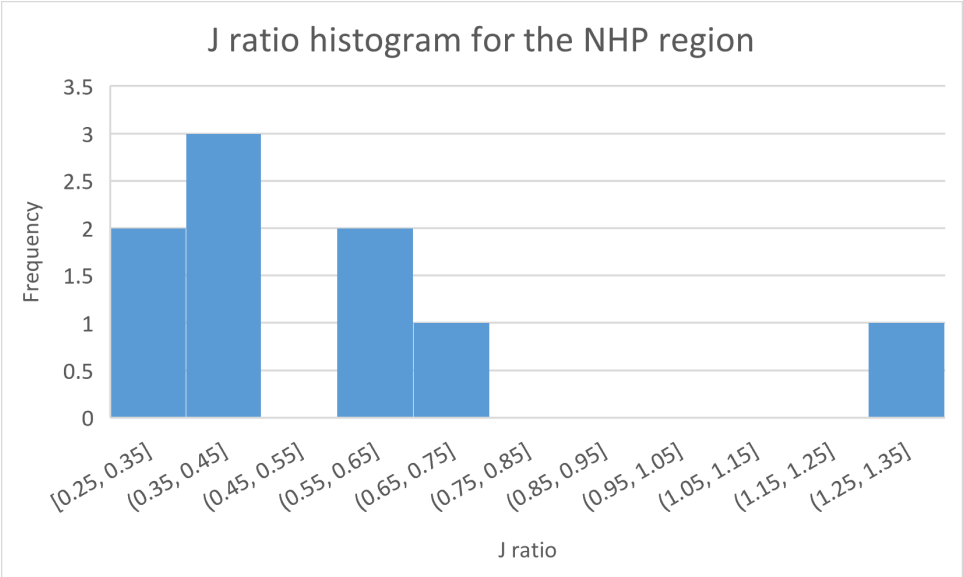

Figure A15: J ratio histogram of NHP

E.2 LTHP

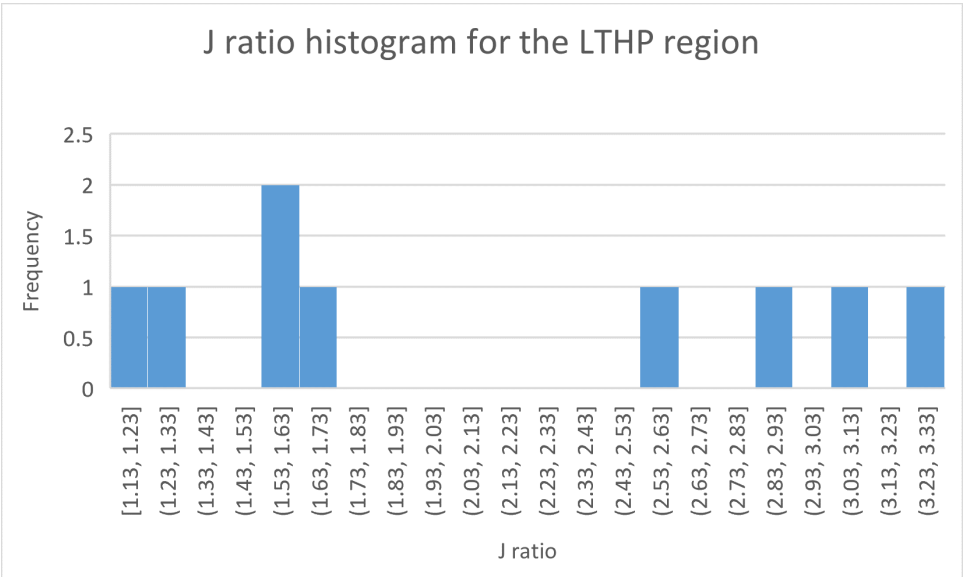

Figure A16: J ratio histogram of LTHP

E.3 GRO

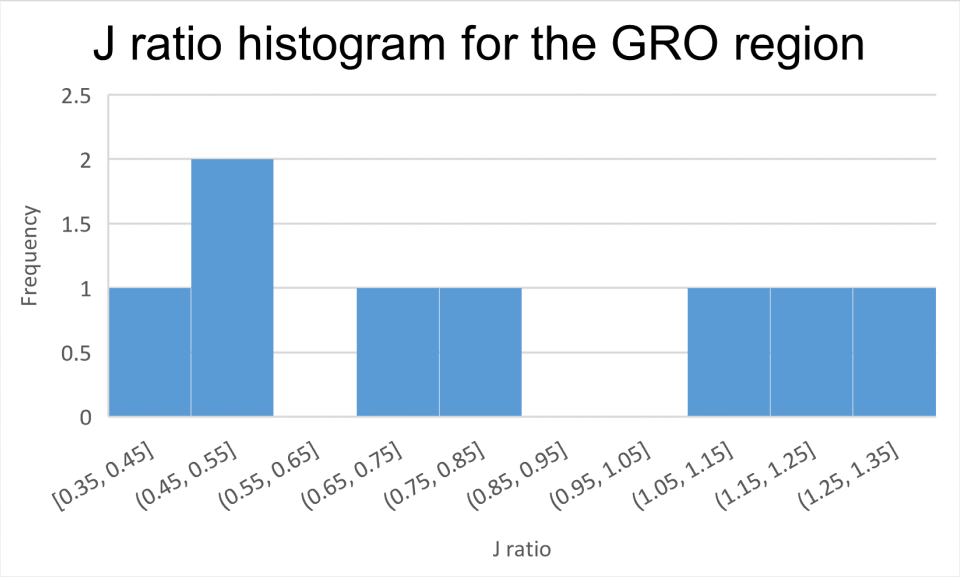

Figure A17: J ratio histogram of GRO

E.4 FP

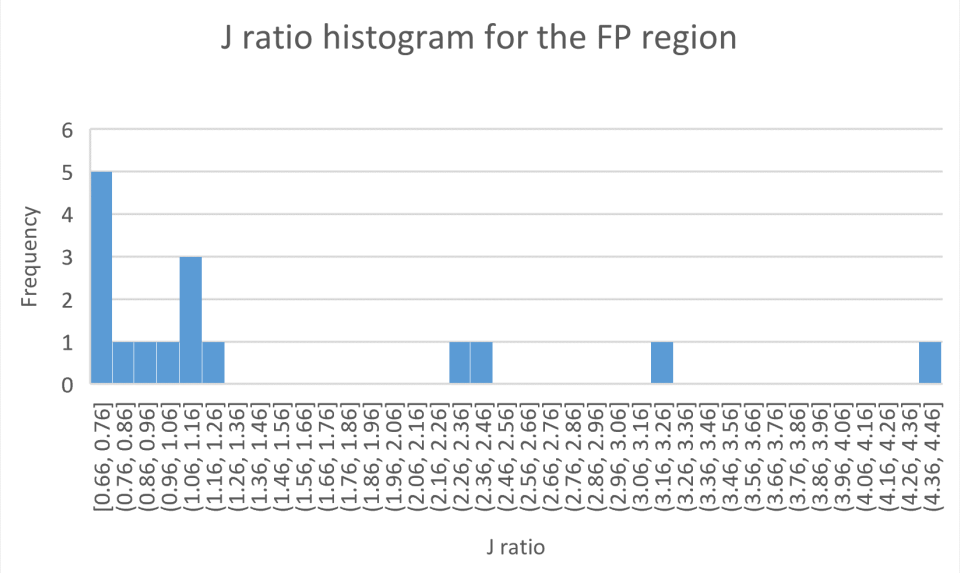

Figure A18: J ratio histogram of GRO

E.5 LT

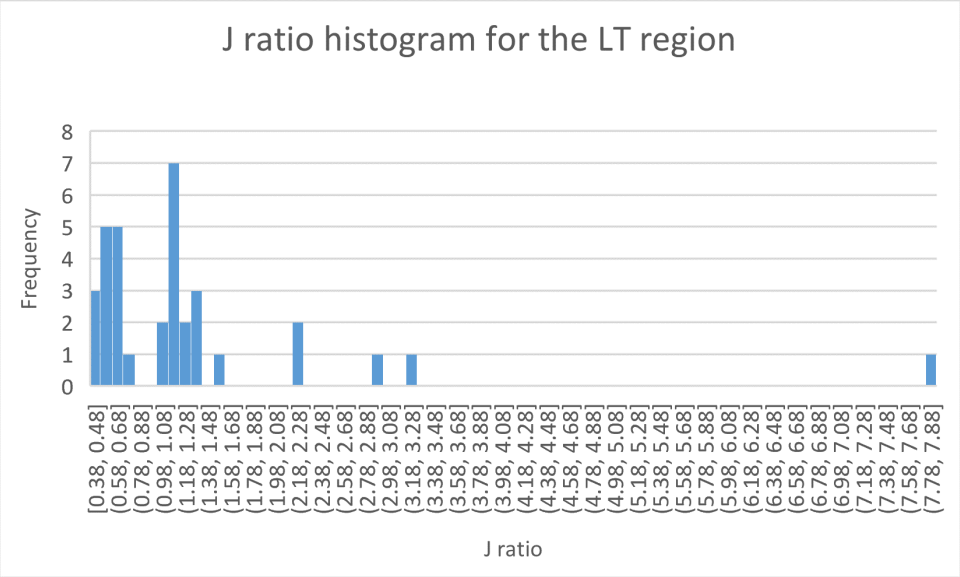

Figure A19: J ratio histogram of LT